UPF1 is required for gene expression in mitochondria and paternal mtDNA clearance during spermatogenesis

Matthew T Wright[1+], Anand K Singh[1,2,3+]*, Hannah L Dixon[1], Emily M Price[1], Elizabeth Connolly[4], Alessandro Di Maio[5], Jonathon Barlow[6], Marco Catoni[1], Yun Fan[1] and Saverio Brogna[1*]

[1]School of Biosciences and Birmingham Centre for Genome Biology (BCGB), University of Birmingham, Edgbaston, Birmingham, B15 2TT, United Kingdom.
[2]Department of Biology, Indian Institute of Science Education and Research (IISER) Tirupati, India, 517619.
[3]Interdisciplinary School of Life Sciences, Institute of Science, Banaras Hindu University, Varanasi, India, 221005.
[4]Department of Biology, Faculty of Science, University of Copenhagen, Universitetsparken 15, Building. 3, 3rd Floor, 2100 Copenhagen O, Copenhagen, Denmark.
[5]Tech Hub Microscopy Facility, College of Medical and Dental Sciences, University of Birmingham, Edgbaston, Birmingham, B15 2TT, United Kingdom.
[6]Cellular Health and Metabolism Facility, School of Sport Exercise and Rehabilitation Sciences, University of Birmingham, Edgbaston, Birmingham, B15 2TT, United Kingdom.

* Correspondance: s.brogna@bham.ac.uk and anandsplash@gmail.com
[+] These authors contributed equally to this work and are considered co-authors.

Abstract

UPF1 is a conserved RNA helicase in eukaryotes which is crucial for the correct expression of nuclear genes. This study presents ChIP-seq evidence indicating its RNA-dependent interaction with mtDNA transcription sites in *Drosophila* S2 cells. Mitochondrial and frequent co-localisation with nucleoids were validated by immunostaining and GFP-tagging in various fly tissues and cell types. Depletion of UPF1, but not other NMD factors, during spermatogenesis, causes severe meiosis and cytokinesis defects, leading to sterility. RNA-seq indicates that these phenotypes could be primarily due to the reduced expression of genes essential for chromosome segregation. Yet also shows that spermatids depleted of UPF1 exhibit a widespread downregulation of mtDNA transcription and, unlike in wild type, fail to eliminate their mtDNA at the elongation stage. Cumulatively, this study indicates a crucial requirement of UPF1 in the expression of both nuclear and mtDNA genes during spermatogenesis.

Key words: UPF1, NMD, mitochondria, mtDNA gene expression, paternal mtDNA elimination, RNA helicases, *Drosophila*

Introduction

UPF1 is an evolutionary conserved RNA helicase of eukaryotes necessary for correct gene expression. This helicase binds both RNA and single-stranded DNA *in vitro* and uses ATP hydrolysis to unfold secondary structures and to displace associated proteins (Bhattacharya *et al*, 2000; Chakrabarti *et al*, 2011; Czaplinski *et al*, 1995; Fiorini *et al*, 2015). UPF1 is typically found in the cytoplasm, where it is associated with mRNA in a translation-dependent manner and it is most prevalent in the mRNA 3′-UTR (Hogg & Goff, 2010; Hurt *et al*, 2013; Zund *et al*, 2013). While UPF1 is better known for its role in nonsense-mediated mRNA decay (NMD) - a translation-linked process that has been described in all eukaryotes, the exact mechanism is still insufficiently understood (Brogna *et al*, 2016; Brogna & Wen, 2009; Fatscher *et al*, 2015; Goetz & Wilkinson, 2017; He & Jacobson, 2015; Hug *et al*, 2016; Karousis *et al*, 2016; Kim & Maquat, 2019; Lykke-Andersen & Jensen, 2015). Recent research has shown that UPF1 rapidly moves between cell compartments, associating with nascent RNA in the nucleus to potentially influence transcription and other processes associated with gene expression in divergent species like *Drosophila melanogaster* and *Schizosaccharomyces pombe* (De *et al*, 2022; Singh *et al*, 2019; Singh *et al*, 2020). The misregulation of UPF1 is linked to several diseases, including neurodegeneration and cancers (Chen *et al*, 2022; Petric Howe & Patani, 2023; Staszewski *et al*, 2023; Zaepfel *et al*, 2021; Zuniga *et al*, 2023). However, it is still unclear whether these diseases are solely caused by the increased stability of NMD-sensitive mRNAs, or are due to specific, NMD-independent functions of UPF1 in gene expression.

The name UPF1 (*UP-F*rameshift-*1*) originates from its identification in a genetic screen for co-suppressors of an up-frameshift mutation in *Saccharomyces cerevisiae* (Culbertson, 1999; Leeds *et al*, 1991). However, this gene was initially characterised as *NAM7* (*N*uclear *A*ccommodation of *M*itochondria *7*) in a screen for nuclear genes that, when overexpressed, restore respiration in strains carrying mutations in Group I or Group II introns of mitochondrial genes (Altamura *et al*, 1992; Asher *et al*, 1989). Deletion of *UPF1*, *UPF2* and *UPF3*, which all equally inhibit NMD, lead to respiratory impairment in *S. cerevisiae*. However, only *UPF1* overexpression can suppress mitochondrial splicing mutations (de Pinto *et al*, 2004). Since UPF1 was not detected in *S. cerevisiae* mitochondria, these effects were therefore interpreted to be a consequence of UPF1 overexpression, resulting in the misexpression of undefined nuclear-encoded proteins involved in mitochondrial splicing (de Pinto *et al.*, 2004). However, the possibility that a small amount of UPF1 may localise in mitochondria to impact mtDNA gene expression could not be ruled out (de Pinto *et al.*, 2004).

In this study, we began with the unexpected discovery that specific regions of mtDNA are significantly enriched by UPF1 ChIP-seq in *Drosophila* S2 cells. ChIP qPCR confirmed its association with mtDNA genes, likely by binding the nascent RNA, as the association is sensitive to RNAase. The mitochondrial localisation of UPF1 was confirmed by immunostaining and GFP-tagging in several *Drosophila* tissues, including the salivary gland and indirect flight muscles, with a detailed focus on spermatogenesis. Throughout spermatogenesis, UPF1 is equally abundant in mitochondria and the cytoplasm, especially in the nebenkern - a distinctive structure formed by the fusion and furling of all mitochondria, located next to the haploid nucleus of the round spermatid (Fabian & Brill, 2012; Hales & Fuller, 1997). Knockdown of UPF1 (UPF1KD) during spermatogenesis, causes abnormalities in meiosis and nebenkern formation, resulting in complete male sterility. However, the knockdown of other NMD factors shows no apparent abnormalities and the flies are fertile.

Additionally, a striking mitochondrial phenotype is seen in UPF1KD elongated spermatids, whereby they retain the mtDNA in their axonemal mitochondria. Whereas, in wild type, this is removed by mechanisms that prevent the inheritance of paternal mtDNA. Before this investigation, the only proteins implicated were the mitochondrial endonuclease EndoG, and mtDNA polymerase POLG1 in *Drosophila* (DeLuca & O'Farrell, 2012; Lee *et al*, 2023; Patel, 2017; Yu *et al*, 2017), and mitochondrial transcription factor A (TFAM) in humans (Lee *et al.*, 2023). This study also provides RNA-seq data that highlights specific misregulated genes in UPF1KD testes, which likely explain the observed failure in spermatogenesis. These data, combined with RNA-seq of additional cell types, indicate that UPF1 is also required in mtDNA expression, which is particularly striking in spermatids. Our data cumulatively envisages a putative novel mechanism of paternal mtDNA clearance which may involve association of UPF1 with mtDNA.

Results

UPF1 is associated with transcription sites and other regions of the mtDNA

Whilst re-analysing UPF1 ChIP-seq datasets generated during an earlier study (Singh *et al.*, 2019), we made the unexpected observation that specific regions of the mtDNA are enriched and could therefore, be directly or indirectly associated with UPF1. The enrichment is most apparent for the A-T-rich of the mtDNA, with the first half showing more enrichment than the second (Figure 1A). This region consists of two arrays of highly similar sequence repeats that can be classified into distinct sequence types, one located in the first half, and the other in the second, which are separated by nonrepetitive sequences (Lewis *et al*, 1994). The A-T-rich region corresponds to the D-loop in mammalian mtDNA, which is also known as the major noncoding region (NCR)(Holt & Reyes, 2012). This, in *Drosophila*, contains a unidirectional mtDNA replication origin in its middle, which advances in the direction of rRNA genes (Joers & Jacobs, 2013). The A-T-rich region is flanked by two promoter/transcription start site (TSS) regions which correspond to two major divergent transcription units, containing a cluster of seven protein-encoding genes (TU1), and the other to the small and large ribosomal rRNAs (TU3) and the ND1 gene (Figure 1A)(Torres *et al*, 2009). The TSS region of the other two divergent transcription units, located between the ND4 and ND6 genes, appear to also be enriched (Figure 1A; TU2 and TU4) (Torres *et al.*, 2009). The enrichment profile is similar between the two biological replicates, despite the different overall levels of enrichment in the two repeats (Figure 1A, top red graphs). Enrichment of mtDNA is not typically detected in ChIP experiments with S2 cells. For example, there is no evidence of enrichment of these, or the other regions in the Ser2 Pol II ChIP-seq dataset, which was generated in parallel, and similarly aligned (Figure S1A). Likewise, the sequencing of the input sample shows uniform coverage along most of the mtDNA, with somewhat lower coverage at the A-T region, likely, due to the repetitive structure (Figure 1A, bottom purple graph). Although this region mostly consists of sequence repeats (Figure 1A, horizontal yellow arrows); it should also be noted that the enrichment peaks mostly map in the inter-repeat regions, particularly in the second half of the A-T region (a prominent peak is denoted by the black vertical arrow in Figure 1A). This, in conjunction with a lack of enrichment of mtDNA in the Pol II ChIP-seq dataset (including published datasets from other laboratories, which were analysed as a control, Figure S1A), strengthen the interpretation that the binding of UPF1 within the A-T region is also specific.

The association with the rRNA loci and the ND4 region was also validated by independent ChIP-qPCRs. These show an enrichment profile comparable to the ChIP-seq (Figure S1B; the A-T region could not be tested as specific PCR primers could not be designed due to the high A/T content of the sequence). Additionally, the association with the ND4 and rRNA regions is RNase-sensitive (Figure S1C). Although the A-T region could not be assessed for RNase-sensitivity, mitochondrial transcription promoters are bidirectional, this region is likely to be highly transcribed from both TU1 and TU3 promoters in the antisense directions. It is feasible that the association of UPF1 with this region is also RNA-dependent. Whether this association could be partially explained by the binding of UPF1 to ssDNA or RNA/DNA hybrids was not investigated. However, neither type of structure is expected to be prevalent in the A-T region of *Drosophila* (Joers & Jacobs, 2013).

Microscopic visualisation of UPF1 within mitochondria

UPF1 could also be detected in mitochondria by immunostaining of S2 cells (Figure 1B). This showed a punctate signal that is most intense in the cytoplasm, yet some of the UPF1 foci are localised within the mitochondria, identified by staining the cells before fixation with a fluorescently conjugated dye which accumulates in the matrix of functional mitochondria (MitoSpy; Material and Methods). Additionally, UPF1 foci within the mitochondria often colocalise with DAPI-stained regions (Figure 1B, panels II-IV, magnified views of a mitochondrion, the arrow point to one of these foci), which are likely to correspond to nucleoids – clusters of multiple mtDNA molecules (Bogenhagen, 2012).

Purification of mitochondrial fractions from S2 cells, followed by western blotting also indicates that a portion of UPF1 is copurifying with cytochrome c oxidase subunit 4 (COX4; a component of the respiratory chain located in the inner mitochondrial membrane). Whereas, α-tubulin is barely detectable, indicating these mitochondrial fractions have minimal cytoplasmic contaminants (Figure S2).

Next, we examined whether UPF1 can be detected in salivary glands, as these are large cells ideal for microscopic imaging. Here it was found that a portion of UPF1 can also be detected within the mitochondria by both immunostaining of endogenous UPF1, and by imaging of a transgenic GFP-tagged UPF1. Immunostaining of endogenous UPF1 shows strong and profuse signals in the cytoplasm, and to a smaller extent, within mitochondria-demarcated COX4 signal, in second instar larval glands (Figure S3A, the inset shows a magnified view of UPF1

signals within a DAPI stained region). The mitochondrial localisation is also apparent in late third instar larval glands (Figure S4B, at this stage of development the cells are replete with large secretory vesicles). The transgenic GFP-UPF1, expressed using the UAS-GAL4 system with the salivary gland-specific GAL4 driver (*FkhGAL4*, Materials and Methods). Which is overexpressed relative to the endogenous protein (Singh *et al.*, 2019), at high magnification displays a dense punctate pattern, with foci of variable size and brightness throughout the cytoplasm. However, GFP-UPF1 foci can also be detected within mitochondria (Figure S4A, panels V-VIII show a strong GFP-UPF1 dot which colocalises with DAPI).

Prominent UPF1 mitochondrial localisation in flight muscles

UPF1 mitochondrial localisation is strikingly prominent in adult flight muscles. These are characterised by distinctive rows of large, tubular, fused mitochondria, located between the myofibrils. Both immunostaining of endogenous UPF1 (Figure 2A), and imaging of transgenic GFP-UPF1 expressed in the muscle (Figure 2B), using the *MhcGAL4* driver (Materials and Methods), shows that UPF1 appears to be relatively more abundant within mitochondria than the cytoplasm. Regions of cytoplasm can be distinguished as spaces between myofibril bundles that are not occupied by mitochondria, such as the region indicated by the dashed yellow rectangle in Figure 2A, panel I-II. Bright dots of the UPF1 signal are often detected within mitochondrial regions that do not stain for COX4 (Figure 2A, panels IV-VI). These possibly correspond to nucleoids, but it could not be verified by DAPI staining in these preparations. The mitochondrial localisation is striking apparent when GFP-UPF1 is expressed alongside the UAS-*mCherry-mito* transgene (see Material and Methods), in which most of the protein appears predominately localised within the mitochondria, with only a small portion present in the cytoplasm (Figure 2B, panels I-II, a representative region corresponding to the cytoplasm is indicated by the yellow dashed region).

UPF1 mitochondrial localisation is dynamic in spermatids

To further investigate UPF1 mitochondrial localisation, and its putative role in mitochondrial function, we examined the *Drosophila* testes. These contain cells with characteristic large mitochondrial structures which are a consequence of major morphological changes during spermatogenesis. Spermatogenesis starts with a germline stem cell, which, after four cycles of mitosis, generates 16 primary spermatocytes, which produce 64 haploid spermatids following meiosis. Both cell types have recognisable mitochondrial structures. These are the mitoball, a

recently described, transient cluster of mitochondria in pre-meiotic spermatocytes (Li *et al*, 2023); and the nebenkern, a large round structure adjacent to the nucleus of round spermatids, which is formed by fusion of all mitochondria within these cells (Figure 3A)(Hales & Fuller, 1997). We first examined the subcellular localisation of endogenous UPF1 by immunostaining testes ubiquitously expressing mito-mCherry as a mitochondrial marker (*ubi-mito-mCherry*) (Lee *et al*, 1988). This shows punctate staining with as much signal in the mitochondria, as in the cytoplasm in most cell types (Figure 3B-D). This can be observed in both the mitoball (Figure 3B), and the nebenkern (Figure 3C). A similar pattern was seen in the axonemal mitochondria of elongating spermatids (Figure 3D). However, UPF1 signals are absent in the axonemal mitochondrial derivatives of fully elongated spermatids (Figure 3E, panels II and IV). These also lacked DAPI foci in their tail (Figure 3E, panel V), consistent with the expectation of paternal mtDNA elimination prior to the full elongation of the spermatid. We also examined the subcellular localisation of transgenic GFP-UPF1 alongside mito-mCherry using the cell-specific driver *bamGAL4*:*VP16* (*bamGAL4*), which starts to be highly expressed in early spermatogonial cells (White-Cooper, 2012). Similar to the endogenous protein, GFP-UPF1 showed a comparable localisation pattern (Figure S5).

This set of observations demonstrate that UPF1 localises to mitochondria in both primary spermatocytes and developing spermatids, and that UPF1 signals are distributed throughout the mitochondria including in the nucleoid regions. The exception is fully elongated spermatids where neither UPF1 nor nucleoid/mtDNA signals are present. It seems, therefore, that the localisation of UPF1 in mitochondria correlates with mtDNA presence in spermatids.

UPF1 is required for chromosome segregation and cytokinesis as well as normal nebenkern assembly

Given the mitochondrial localisation of UPF1 in the nebenkern, we examined what the consequences of knockdown would be for the developing spermatids, as the nebenkern is required for the correct development of mature spermatids (Noguchi *et al*, 2011). In wild type, the nebenkern is found adjacent to the nucleus of the round-stage spermatid (Figure 4A, panel I). However, in UPF1KD (knocked down by *bamGAL4*-driven RNAi) testes at this stage, most nuclei lack the adjacent nebenkern, between the four haploid spermatids there is a single, abnormal, giant nebenkern (Figure 4B, panels I-III). Although, a syncytium-like appearance can also frequently be observed in wild type with this type of preparation (Figure 4A, panel II), consistent with previous reports (Hales & Fuller, 1997), groups of four distinguishable round

spermatids were not observed in UPF1KD testes. Therefore, the syncytium appearance, and the formation of a single giant nebenkern is likely a consequence of incomplete cytokinesis, and the fusion of all mitochondria from all four spermatids. Additionally, the nuclei of different sizes suggest chromosomal segregation defects, as previously reported for meiotic mutants (Giansanti & Fuller, 2012; Giansanti *et al*, 2012).

Quantification of the nebenkern area in wild type and UPF1KD spermatids reveals that the two-dimensional area of the nebenkern in UPF1KD spermatids is approximately 3.3-fold larger than that of wild type round spermatids (Figure 4C). Implying that the volume is more than 4-fold greater than that of a normal nebenkern. As a result, it is likely much less compact, consistent with its appearance (Figure 4A vs 4B). This giant nebenkern shows additional structural abnormalities, including spheroid bodies within the giant nebenkern (Figure 4B, indicated by arrowheads in panel III). These have the appearance of membrane-bound vacuole-like compartments. These are similar to those previously described in spermatogenesis mutants which affect nebenkern formation (Dorogova *et al*, 2013), which could potentially represent cytoplasmic inclusions. However, the spheroid-bodies that have been described here seem larger. Additionally, these bodies are not destroyed by the pressure applied during the testes squashing preparation procedure, indicating that they must be bound by a stiff membrane or double membrane enclosure. It is not likely they are nuclei though, as they do not appear to contain DNA (Figure S6). Additionally, no MitoTracker (mitochondrial dye similar to MitoSpy) signal can be detected within (Figure S6), perhaps suggesting that these bodies are large mitochondrial-fusion derivatives that no longer have functional polarised membranes. In size and shape, they are reminiscent of the enigmatic giant mitochondria observed by TEM in human pathologic cells (Shami *et al*, 2023).

Additionally, structural differences between the nebenkern in wild type and UPF1KD have been observed. First, two different types of nebenkern can be distinguished in round onion-stage spermatids in wild type (Figure S7A). As far as we are aware, this has not been described in the literature. The first, likely early-stage, displayed an oblong shape, in which there are visible layers of the mitochondrial derivatives (Figure S7A, panels I-III). The second, late-stage, was round, lacking visible layering (Figure S7A, panels IV-VI). These stages of nebenkern could not be distinguished in UPF1KD though (Figure S7B). Notably, it appears that there is 1.5-fold more DNA (corresponding to the corrected total DAPI fluorescence signal within the nebenkern region; see Material and Methods) in the late-stage compared to the early-

stage (Figure S7C), consistent with mtDNA replication occurring during nebenkern formation, as implied by previous observations (Yu *et al.*, 2017). In the UPF1KD nebenkern, there is 5.38-fold and 3.45-fold more mtDNA compared to the early and late nebenkern in wild type, respectively (Figure S7C). This is consistent with the giant nebenkern likely deriving from the fusion of mitochondria from four, insufficiently separated, spermatids. Notably, protruding structures often containing DNA were observed at the periphery of the apical side of late-stage nebenkern in wild type (Figure S7D, panel I-IV). However, no such structures were found in the UPF1KD nebenkern, nor is there DNA in the large spheroid bodies present within, as described above (Figure S7B, panel III; Figure S6). These protrusions could represent an intermediate stage of a potential mechanism that expels mtDNA, similar to the extrusion of mtDNA during the cGAS-STING pathway, an innate immune response which triggers inflammation in response to cytosolic mtDNA (Kim *et al*, 2023; Riley & Tait, 2020); we have not characterised their frequency and significance in mtDNA clearance.

UPF1 depletion but not that of other NMD factors causes male sterility

We evaluated the fertility of flies depleted of UPF1, and other NMD factors during spermatogenesis using *bamGAL4*-driven RNAi. UPF1KD using two independent RNAi lines (see Materials and Methods) showed complete male sterility, while that of UPF2KD, and UPF3KD resulted in fertile males (Figure 5A). SMG5KD also did not affect male fertility (unpublished data). The sterility can be explained by the absence of mature sperm. In wild type, the seminal vesicle is full of mature sperm (Figure 5B, Panels I-III), however, in UPF1KD testes none is observed (Figure 5B Panels, IV-VI, RNAi$^{(1)}$; and Figure 5C, panels I-III, RNAi$^{(2)}$). Inversely, sperm is detected in the seminal vesicle of UPF2KD and UPF3KD testes (Figure 5C, Panels IV-IX). Since no mature sperm is produced, the cysts containing the elongated spermatids must be eliminated before entering the seminal vesicle in UPF1KD.

UPF1 is required for normal expression of genes involved in chromosome segregation

To gain insight into the genetic mechanism responsible for the spermatogenesis phenotypes, we performed RNA-seq of UPF1KD testes, using *bamGAL4*-driven expression of both UPF1 RNAi lines, alongside wild type testes. Differential gene expression analysis of these samples shows broad misexpression of genes. We found that out of the 23,793 genes expressed, 3,218 are misregulated (Figure S8), corresponding to approximately 14%. This was unexpected, for example, only a total of 214 and 1,901 genes are misregulated in UPF1KD, in S2 and salivary gland cells, respectively (based on RNA-seq data described below). This is similar to what was

observed in previous studies (Brooks *et al*, 2015; Chapin *et al*, 2014; Rehwinkel *et al*, 2005). Gene ontology (GO) analysis of all misregulated genes, identified in testes, did not reveal an enrichment of any specific GO set. With the notable exception that five of the top ten upregulated genes all encode proteins which are normally encoded in the male accessory glands and transferred to the females after copulation (Figure S8). This is unexpected (and so far, unexplained), as the accessory glands were carefully removed during the dissection and the *bamGAL4*-driven RNAi is not expressed in these cells.

When focusing the analysis on the known genes predicted to be involved in spermatogenesis (507), 53 genes are misregulated, 40 upregulated, and 13 downregulated (Figure 6). Notably, GO classification shows that mostly all of the downregulated genes are involved in interconnected functions related to chromosome segregation (Figure 6D). Three genes are particularly overrepresented in these sets. One of them is Mps1 ($\log_2$ fold change (LFC): -1.01, adjusted P-value (*P.adj*): 1.47E-06), a master regulator of the spindle assembly checkpoint (Moura *et al*, 2017). The other two are *asunder* (*asun;* LFC: -1.47, *P.adj*: 1.11E-04) and *Dynactin-1* (*DCTN1-p150*; LFC: -1.15, *P.adj*: 8.22E-15), which encode proteins required for the interaction between the dynein–dynactin microtubule motor complex and the kinetochore (Anderson *et al*, 2009; Holzbaur *et al*, 1991). Mutations in these genes result in chromosome segregation and cytokinesis phenotypes similar to those we have described above during spermatogenesis in the UPF1KD. It is feasible that the 2-3-fold downregulation of one or more of these genes could potentially explain the abnormal chromosome segregation and the cytokinesis phenotypes. As for the genes that are upregulated, the GO analysis shows enrichment of gene sets involved in mid to late spermatogenesis, such as sperm individualisation, and spermatid differentiation, and it also included genes required for apoptosis (Figure 6C). However, rather than reflecting changes in gene regulation, it could be a consequence of the spermatogenesis delay, resulting in an increase in the number of spermatids that may be entering this later stage of differentiation in the UPF1KD testes relative to wild type. As no mature sperm are produced, cysts containing such aberrant spermatids could be eliminated by a process similar to that which eliminates spermatids with damaged DNA, thereby protecting genomic integrity (Lu & Yamashita, 2017).

UPF1KD results in paternal mtDNA retention

Despite the major disruption in spermatogenesis, elongated spermatids are produced in UPF1KD testes (Figure S9). These incorporate GFP-tagged Don Juan (Figure S9), a marker of

elongating, and fully elongated spermatids (Santel *et al*, 1997). Notably, unlike in wild type, multiple clusters of DAPI signal could be detected and evenly distributed throughout the spermatid tails in UPF1KD; the bundle of spermatids we have compared appear to be at a similar developmental stage, based on nuclei morphology (Figure 7, panels III-IV). The DAPI signals in UPF1KD likely represent mtDNA/nucleoids, which are absent in wild type, at a similar stage of elongation (Figure 7, panel I and II). Given the apparent defects in chromosomal segregation described above, it was considered whether these could instead be fragments of chromosomal DNA. To distinguish between these two explanations, we utilised a transgene expressing GFP-tagged TFAM, as a marker of mtDNA (*BAC-TFAM-GFP*, see material and methods). This examination showed that TFAM-GFP is weak and diffuse in wild type mature sperm tails relative to that in round spermatids (Figure S10, panels I and IV-V), while TFAM-GFP signal is brighter in the UPF1KD tails, which, at higher magnification, appears as dots that colocalise with DAPI signals throughout the entire tail in UPF1KD spermatids (Figure S10, panels IX-X). These observations are consistent with the DAPI staining and indicate that this phenotype is specific to UPF1KD as no evidence of TFAM/mtDNA foci was observed in either UPF2KD or UPF3KD spermatids (Figure S10, RNAi efficiency of each line was experimentally verified, see figure legend).

The mtDNA copy number was also quantified by qPCR in wild type, and UPF1KD testes using either of the two RNAi lines described above. This analysis indicates that UPF1KD testes carry 3-fold or more mtDNA compared to wild type (relative to the autosomal genomic locus: *RpL32*). This increase is apparent in pre-eclosed and eclosed males, with a greater increase seen in the eclosed males (Figure 7B and C, respectively). However, in UPF1KD salivary glands (Figure 7D) and S2 cells (Figure 7E), there is no change to the number of mtDNA copies relative to wild type. Therefore, all the data seem consistent with the interpretation that these dots correspond to mtDNA/nucleoids that are retained in the UPF1KD elongated spermatid tail.

Reduced expression of mtDNA genes in UPF1KD spermatids and other cell types

Following the assessment of genes required for spermatogenesis, the testes RNA-seq datasets were analysed for differential expression of the known mitochondrial genes. This analysis revealed that 71 genes of 912 are misregulated, 40 upregulated, and 31 downregulated (Figure 8A). The first notable observation is that 11 of the downregulated genes are mtDNA-encoded genes (Figure 8B). The most significantly downregulated gene is *ND4* (LFC: -1.43, P.adj:

2.51E-18). Next, it was considered whether these changes could be attributed to the downregulation of genes encoding the proteins required for mitochondrial transcription. Both upregulated and downregulated mitochondrial-associated genes were analysed for GO enrichment. Notably, the upregulated set shows the enrichment of genes involved in mitochondrial transcription, rather than their downregulation (Figure 8C-D). Specifically, three of the four genes involved in mitochondrial transcription are upregulated (*mtRNApol*, *mTFB2,* and *mTerf3*), with only *TFAM* being downregulated (Figure 8E). Other upregulated genes include several proteins involved in mitochondrial energy metabolism, such as Cyp12d1-Cytochrome P450 12d1 (*Cyp12d1-d*), Glycerol kinase 2 (*Gk2*), Complex I intermediate-associated protein 30 kDa (*CIA30*), and glutaryl-CoA dehydrogenase (*ETF, CG9547*).

In addition to the mtDNA genes, the other downregulated genes encode proteins involved in mitochondrial translation, with most of them encoding mitochondrial ribosomal proteins (Figure 8D). Two other genes that are downregulated include an essential component of the TIM23 complex: *Tim17a2,* and *scheggia* (*sea*) which encodes a carrier protein that plays a central role in fatty acid and sterol biosynthesis. As for mtDNA elimination, the expression level of the two currently known Drosophila genes involved in the process differs, *EndoG* is downregulated, but *PolG1* is upregulated (Figure 8F).

To investigate whether UPF1 could potentially affect mtDNA gene expression in other cells, first, we performed RNA-seq of UPF1KD S2 cells and, as control the other NMD factors (UPF2KD and UPF3KD). The analysis revealed that 11 of the 912 mitochondrial-associated genes were misregulated, and all of them were upregulated (LFC >1; Figure S11). However, closer inspection of the mtDNA genes revealed that six out of the 15 mtDNA genes are also significantly downregulated in UPF1KD S2 cells (Figure S11A). Although the downregulation is modest compared to what is seen in spermatids (between -0.2 and -0.3 LFC), the adjusted P-value indicates significant misregulation (P.adj ≤0.005). These six downregulated genes show a greater UPF1 ChIP association than other mtDNA genes in S2 cells, with *ND4* demonstrating the greatest downregulation (LFC: -0.29/-0.30; P.adj: 4.89E-03), like in spermatids. No significant changes in the expression of mtDNA genes were detected in UPF2KD or UPF3KD S2 cells (Figure S11B and Figure S11C). Additionally, there is no evidence of downregulation of genes involved in mitochondrial transcription in UPF1KD. As observed in testes, *mTerf3* is upregulated (Figure S11A, bottom panel). We also performed this analysis on RNA-seq of salivary glands. Similar to what is seen in the other datasets, several genes show a trend of

downregulation (-1.5 > LFC), with four genes having a *P.adj* around 0.05 (Figure S12A). While these changes are less statistically significant than in S2 cells and testes, RNA-seq of UPF2KD and UPF3KD salivary glands shows no evidence of mtDNA transcription downregulation (Figure S12B and S12C). Instead, UPF2KD salivary glands show upregulation of two mtDNA genes (Figure S12B). Also, in this instance, the downregulation is unlikely due to misregulation of the genes required for mtDNA transcription, as none of these genes are downregulated. Instead, *mtTFB2* and *mTerf3* are upregulated, in UPF1KD, and *mTerf3* is also upregulated in UPF2KD and UPF3KD salivary glands (Figure S12A-3C, bottom panels).

The downregulation in mtDNA gene expression is also not linked to changes in mtDNA copy number, as this is unchanged in the UPF1KD samples examined in the testes, S2 cells, and salivary glands (Figure 7B-E).

In summary, the most apparent change revealed by RNA-seq of UPF1KD is a reduction in the expression of the mtDNA genes. This was observed in different types of cells and is strikingly apparent in spermatids.

Discussion

We have provided evidence that the RNA helicase UPF1 enters mitochondria and becomes associated with mtDNA. This conclusion is drawn from several experimental observations, including ChIP-Seq data from *Drosophila* S2 cells, revealing an association with mtDNA transcription sites and possibly also with the major noncoding region. At the gene sites, the association is most apparent at promoter-proximal regions of the transcription units and likely reflects an association with nascent RNA, as indicated by RNase-sensitive ChIP-qPCR experiments. UPF1 was also visually detectable in mitochondria via immunostaining, and by the expression of a transgenic GFP-tagged variant in different *Drosophila* cell types. In most cells examined, UPF1 is less abundant in mitochondria compared to the cytoplasm. However, in muscles, a higher level of UPF1 was observed in the mitochondria than in the cytoplasm, and in spermatids, the level in the mitochondria is like that of the cytoplasm.

This was unexpected, as UPF1 sequence lacks an N-terminal mitochondrial targeting signal (MTS) and is not predicted to localise to mitochondria by computational methods, based on published data (Chacinska *et al*, 2009; Fukasawa *et al*, 2015; Savojardo *et al*, 2020). However, this is not unusual, as several core mitochondrial proteins do not possess an MTS, and their localisation cannot be predicted from the primary sequence (Bader *et al*, 2020). For example, about 25% of yeast mitochondrial ribosomal proteins (MRPs) do not possess a classic MTS (Bykov *et al*, 2022). UPF1 could be categorised as a dual-localised protein, or even more accurately, given its localisation in the nucleus and the cytoplasm, a tri-localised protein.

As mitochondrial reorganization plays a crucial role in spermatids development and UPF1 localisation is particularly apparent in the nebenkern, we have focused on spermatogenesis. Our data show that UPF1 is essential for spermatogenesis, and this is independent of its role in NMD, as other NMD factors UPF2 and UPF3 (as well as SMG5, data not shown) did not affect spermatogenesis. This conclusion differs from that of previous studies which have concluded that NMD is required for spermatogenesis in mice, and other organisms (Bao *et al*, 2016; Fanourgakis *et al*, 2016; Han *et al*, 2018; Lehtiniemi *et al*, 2022). Many of the abnormalities observed in spermatids could account for sterility, including abnormal chromosomal segregation and incomplete cytokinesis during meiotic cell division. Despite this, some elongated spermatids are generated, and probably 25% of the expected number is generated, which is consistent with the nebenkern being necessary for elongation (Noguchi *et al.*, 2011). Yet, as no mature sperm cells are observed in the seminal vesicle, these abnormal elongated

spermatids must be eliminated at a later stage, perhaps by the fusome which may eliminate these due to their variable genomic content (Lu & Yamashita, 2017).

Mitochondrial phenotypes were also observed in UPF1KD, the most striking is that spermatids fail to remove their mtDNA at the late stages of the development. To gain insight into what the role of UPF1 might be in mtDNA expression, as well as understanding the other spermatogenesis phenotypes, we have performed a number of RNA-seq experiments with the testis and other cell types. In testes, these identified significant downregulation of three genes that could potentially explain the spermatogenesis defects. These are *Mps1*, a master regulator of the spindle assembly checkpoint (Moura *et al.*, 2017). The other two are *asunder* and *Dynactin-1* which encode proteins required for the attachment of the dynein–dynactin complex to the kinetochore (Anderson *et al.*, 2009; Holzbaur *et al.*, 1991). Mutations in these genes result in spermatogenesis phenotypes similar to those we have observed. Given that depletion of the other NMD factors does not affect spermatogenesis, and that UPF1 is known to associate with nascent RNA of Pol II transcribed genes, in *Drosophila* as well as fission yeast (De *et al.*, 2022; Singh *et al.*, 2019), it can be envisaged that UPF1 is a positive regulator the expression of these genes directly in the nucleus.

An additional result of the RNA-seq experiment is that most of the mtDNA genes (11 of the 15 analysed) are significantly downregulated in the UPF1KD spermatids. Downregulation of mtDNA genes was also seen in the other cell types examined, S2 cells and salivary glands, although not to the same extent as spermatids. The downregulation of mtDNA genes is not observed when other NMD factors are depleted. Moreover, there seems to be a correlation between the UPF1 ChIP association and the level of downregulation. Based on these data and the evidence for UPF1 association with mtDNA transcription sites, it is plausible that UPF1 plays a direct role in mtDNA gene transcription or transcription-coupled processes. Transcription downregulation might result in reduced/abnormal association of factors that could potentially be involved in mtDNA elimination. There is some evidence of a connection between transcription downregulation and the association of TFAM to mtDNA in *Drosophila* (Wang *et al*, 2021), and inhibition of TFAM import to the mitochondria is linked to mtDNA elimination from human spermatozoon (Lee *et al.*, 2023). Our data would predict a positive role of transcription in mtDNA elimination. Whether transcription/UPF1 is required for the recruitment of the already known factors required for paternal mtDNA elimination, EndoG,

and POLG1, as reported in *Drosophila* (DeLuca & O'Farrell, 2012; Yu *et al.*, 2017), remains to be investigated.

In conclusion, our data show that the primary reason for the failure of spermatogenesis in UPF1KD is likely linked to the downregulation of specific nuclear genes essential for chromosome segregation and cytokinesis during meiotic cell division. These data also demonstrate an unanticipated role for UPF1 in the elimination of mtDNA from the sperm cell, which could be linked to its association with mtDNA and requirement in mtDNA transcription.

Materials and Methods

Cell Culture, RNAi interference and immunostaining

S2 cells (CVCL_Z232) were cultured in Schneider's insect cell culture media (Catalogue number: ESF291, Generon) supplemented with 10% Fetal Bovine Serum (FBS), and 1% Penicillin-Streptomycin-Glutamine mix (P/S/G, Invitrogen) at 27ºC. RNAi constructs for UPF1 were amplified by PCR using primers for the desired sequence in addition to the T7 promoter sequence at their 5' end (bold) (5'-**TTAATACGACTCACTATAG**GGGAGA-3'). The PCR product was purified using the Monarch PCR and DNA cleanup kit (T1030S, NEB) and dsRNA was synthesised using the T7 RiboMAX express system (P1700, Promega). In a 6-well plate, 10^6 cells were seeded in each well, incubated overnight, and then treated with 15 µg of dsRNA per well, in serum-free media. The cells are incubated for 1 hour at room temperature before being supplemented with 2 mL of complete media. The cells were incubated for three days to knockdown the UPF1 mRNA, before being harvested. For immunostaining, S2 cells (1 mL corresponding to about 10^6 cells) were seeded onto Concanavalin-A (500 µg/mL) treated coverslips, in a 6-well plate for 30 minutes at 27ºC to allow attachment. Excess media was eluted off and replaced with serum-free media containing typically 250 nM MitoSpy™ Red CMXRos (424801, BioLegend)(in some experiments MitoTracker was used instead, as indicated in the figure legends; MitoTracker™ Red CMXRos, M7512, ThermoFisher Scientific). The cells were incubated with MitoSpy for 30 minutes at 27 ºC, protected from light. Cells were then washed twice in serum-free media, fixed for 15 minutes in 4% paraformaldehyde at room temperature, washed twice in 1X PBS (13 mM NaCl, 0.7 mM Na_2HPO_4, pH 7.4), permeabilised for 15 minutes at room temperature in 0.1% PBT (1X PBS, 0.1% Triton X-100 T8787, Sigma-Aldrich), and blocked for 1 hour at room temperature in blocking solution (5% Bovine Serum Albumin (BSA), 0.05% sodium azide, and 1X PBS). They were then incubated in primary antibody for 16 hours at 4ºC, washed and incubated in the appropriate, fluorophore-conjugated secondary antibody for 2 hours at room temperature. After incubation with antibodies, samples were washed in 1X PBS and incubated with DAPI (4-6-diamidino-2-phenylindole, Sigma-Aldrich, 1 µg/mL) for 10 minutes at room temperature. Samples were briefly washed in 1X PBS and mounted in VectaShield® antifade mounting medium (Vector Laboratories).

Drosophila stocks and husbandry

Flies were reared on standard cornmeal fly food media at 25ºC. The *y* w^{118} strain was used as wild type (DGGR_108736). The following lines were obtained from Bloomington *Drosophila* stock centre: *UAS-GFP-Upf1* (24623), *UAS-Upf1*^{HMC05537} (referred to as UPF1$^{RNAi(1)}$; 43144), *UAS-Upf1*^{GL01485} (referred to as UPF1$^{RNAi(2)}$; 64519), *UAS-mCherry-mito* (66533), *UAS-Upf2*^{JF01560} (31095), *UAS-Upf3*^{HMJ22158} (58181), and *UAS-dj-GFP* (5417). The following *Gal4* drivers *forkhead* (*Fkh)*(Henderson & Andrew, 2000), *myosin heavy chain* (*Mhc*)(Schuster *et al*, 1996), *bag-of-marbles* (*bam*)(White-Cooper, 2012), drove expression of UAS constructs within the salivary glands, muscles, and late spermatogonia/early spermatocytes, respectively. *BAC-TFAM-GFP* is controlled by the endogenous promoter within a BAC clone derived transgene (Zhang *et al*, 2016) and *ubi-mCherry-mito* is a transgenes controlled by the Ubiquitin promoter (Lee *et al.*, 1988). Combination stocks of second and third chromosomal transgenes were generated through standard combination crosses with a double balancer line (*w; IF/CyO-Act>GFP; MKRS/Tm6, Tb)*.

Antibodies

Antibodies used for immunostaining: rabbit anti-COX4 (COX4I1, NB110-39115, Bio-Techne, diluted 1:100). The mouse monoclonal anti-UPF1 antibodies used was typically 7B12 or in some instances 1C13 (diluted 1:100). The same anti-UPF1 antibodies were used in ChIP-seq as described previously, Singh et al., 2019.

S2 Cell fractionation and western blotting

To isolate the nuclear and cytoplasmic fractions, 2×10^6 S2 cells were harvested and washed twice with ice-cold 1X PBS. Cells were resuspended in 1 mL ice-cold buffer AT (15 mM HEPES pH 7.6, 10 mM KCl, 5 mM MgOAc, 3 mM $CaCl_2$, 300 mM Sucrose, 0.1% Triton X-100, 1 mM DTT, 1X PhosSTOP (4906845001, Roche), 1X cOmplete, Mini, EDTA-free Protease Inhibitor Cocktail (04693159001, Roche) and 1 U/mL Ribolock RNase Inhibitor) and incubated on ice for 10 min as a hypotonic treatment. Cells were lysed using a 2 mL Dounce homogenizer by applying 30-40 strokes with the tight pestle at 4°C. Lysates were divided into two aliquots of 500 µL and each aliquot was layered over 1 mL cushion of buffer B (15 mM HEPES-KOH at pH 7.6, 10 mM KCl, 5 mM MgOAc, 3 mM $CaCl_2$, 1 M sucrose, 1 mM DTT, 1X cOmplete, Mini, EDTA-free Protease Inhibitor Cocktail). Following the centrifugation at 8000 RPM for 15 min at 4°C, the top layer (300 µL) was collected as cytoplasmic fraction. The

pellet was resuspended in 500 µL AT buffer and layered over again on buffer B. Following the centrifugation, the pellet was collected as nuclear fraction. Proteins fractions were analysed by standard western blotting.

Adult and larval tissue immunostaining

Internal organs of third instar larvae were dissected in 1X PBS, fixed for 20 minutes at room temperature in 4% paraformaldehyde (methanol-free; 43368.9L, VMR international), washed twice in 1X PBS, and permeabilised in 0.1% PBT (1X PBS, 0.1% Triton X-100). Samples were incubated in blocking solution for 2 hours at room temperature, antibody incubation, and sample mounting remain the same as mentioned above.

Testes of 2–5-day old adult males were dissected in 1X PBS. The only notable changes compared to larval tissue was a fixation time of 30 minutes at room temperature on a rocker, and one hour permeabilization following fixation in 0.3% PBT (1X PBS, 0.3% Triton X-100) at room temperature. All other steps remained the same as mentioned prior. Testes squash preparations were prepared as described previously (Singh & Lakhotia, 2024)

Female muscle dissection followed a previously established protocol (Tenenbaum & Gavis, 2016), the samples were mounted in the same mounting media as mentioned for the prior cell and tissue samples.

Confocal imaging and image analysis

The images of developing spermatids and nebenkern structure were captured under the phase contrast microscopic setting using x63, 1.4-NA oil immersion objective of Nikon Eclipse 80i fluorescence microscope. Confocal z-stack images of mounted samples were acquired using the Zeiss LSM900 with AiryScan2 module, Zeiss LSM710, Leica TCS SP8 STED, and Leica TCS SP2-AOBS confocal microscopes using Plan-Apo 10X, 25X, 63X, 1.4-NA objectives. All objectives, except for 10X, were oil immersion. Images were processed and quantified using FIJI (Schindelin *et al*, 2012).

Quantification of Total Corrected Fluorescence (TCF) was calculated using FIJI (Schindelin *et al.*, 2012). A mean intensity projection of multi-z-stack image was generated, a region of interest was defined, and then the measure function was used. This was repeated for a

background region to identify the mean of background fluorescence (MBF). The output was inserted into the following formula: TCF = Integrated Density – (Area * MBF).

ChIP-seq

Chromatin immunoprecipitation (ChIP) experiments were performed as previously described, (Singh *et al.*, 2019). Briefly, S2 cells (2 x 10^7) were washed and fixed in 1% formaldehyde (EM grade, Polyscience) for 10 minutes at room temperature. Cross-linking was stopped by addition of 125 mM Glycine for 5 minutes at room temperature. Cells were briefly centrifuged at 4ºC, and rinsed in 1X PBS containing 1X cOmplete, Mini, EDTA-free Protease Inhibitor Cocktail. The pellet is resuspended in lysis buffer (5 mM PIPES pH 8.0, 85 mM KCl, 0.5% NP-40) supplemented within the same protease inhibitor cocktail and 1X PhosSTOP. Cells were centrifuged again, and rediluted in nuclear lysis buffer (50 mM Tris pH 8.0, 10 mM EDTA, 1.0% SDS) with protease inhibitor cocktail and PhosSTOP. The cell suspension is diluted with IP dilution buffer (16.7 mM Tris pH 8.0, 1.2 mM EDTA, 167 mM NaCl, 1.1% Triton X-100, 0.01% SDS). They were sonicated for 5 cycles 30s ON/OFF in a Bioruptor sonicator (Diagenode). Samples were centrifuged; clear supernatant is transferred to a 15 mL tube. Aliquot of supernatant was kept for input DNA extraction. Supernatant diluted with IP dilution buffer. Antibody was added to supernatant and incubated overnight on a rocker at 4ºC. Pre-washed DynaBeads were added to the mix and incubated for 1 hour at 4ºC on a rocker. Beads were washed with low salt buffer (0.1% SDS, 1% Triton X-100, 2 mM EDTA, 20mM Tris pH 8.0, 150 mM NaCl), high salt buffer (0.1% SDS, 1% Triton X-100, 2 mM EDTA, 20 mM Tris pH 8.0, 500 mM NaCl) and 1X TE buffer (10 mM Tris pH 8.0, 1 mM EDTA). Beads are then incubated with elution buffer (0.1 M $NaHCO_3$, 1% SDS) at room temperature for 15 minutes and eluted chromatin was reverse cross-linked by adding de-crosslinking buffer (2 M NaCl, 0.1 M EDTA, 0.4M Tris pH 7.5), and incubated at 65ºC overnight on a rotator. Proteinase K (50 mg/mL) was used to digest proteins, for 2 hours at 50ºC on a rocker. DNA was isolated with a Monarch PCR and DNA Cleanup kit. Sequencing and library prep information was previously described (Singh *et al.*, 2019).

ChIP-seq analysis

UPF1 and Ser2 RNA Polymerase II ChIP-seq datasets (GEO: GSE116806) were initially analysed as previously described (Singh *et al.*, 2019). Additional analysis was done with Polymerase II ChIP-seq public datasets (Nechaev *et al*, 2010)(GEO:GSE18643). Files were

trimmed using TRIMMOMATIC (v0.39)(Bolger *et al*, 2014) to remove low quality reads, and adapter sequences. Output files were aligned to the genome using Bowtie2 v2.5.1 after the construction of a Bowtie2 index of *D. melanogaster* genome BDGP6.46 (Ensembl release 111). The aligned SAM files were converted to BAM files which were sorted and indexed using SAMtools v1.19.2. BAM files were converted to BEDgraph files for visualisation in the genome browser IGV (Robinson *et al*, 2023) using the command genomeCoverageBed command and the options -bga and -ibam from the deepTools v3.5.2 suite (Ramirez *et al*, 2014).

Genomic DNA extraction and quantification

In all instances of genomic DNA (gDNA) extraction, the GeneJET Genomic DNA Purification Kit (K0721, ThermoFisher Scientific) was used. For tissue samples, 20 samples were dissected in triplicate in 1X PBS, centrifuged briefly and PBS eluted off. S2 cells (2×10^7) were centrifuged to form a pellet and washed twice, briefly with 1X PBS. Following the centrifugation and removal of the supernatant from samples, extraction was performed using the protocol recommended for: Mammalian Tissue and Rodent Tail Genomic DNA Purification Protocol. Tissue samples were homogenised with pestles after pelleting to the bottom of the tube by centrifugation, whilst S2 cells were resuspended in the kit-provided digestion solution, directly. A minimum of two hours was allowed for digestion of the sample, testes samples required a longer incubation of 5 hours for complete dissolution. At this point DNA was purified as described in the kit protocol.

To assess mtDNA copy number, extracted gDNA was diluted 1:50 in nuclease-free dH_2O, prior to addition to the qPCR reaction. Each reaction consisted of 3 µL of a primer mix (final concentration of 400 nM), 2 µL of diluted gDNA and 5 µL qPCRBIO SyGreen Blue Mix Hi-ROX (PB20.16-50, PCR Biosystems Ltd).

RNA extraction and quantification

Testes were dissected in 1X PBS, and transferred into ice-cold 1X PBS, the tissue was centrifuged at 1000 g for 30 seconds, the supernatant eluted off, and directly resuspended in 1 mL TRIzol™ Reagent (15596029, ThermoFisher Scientific). Tissue was incubated for 15 minutes at room temperature, vortexed for 1 minute, and 200 µL chloroform was added. Tubes were inverted by hand for 15 seconds until there was a homogenous suspension. Samples were centrifuged for 20 minutes at 15 000 g at 4°C. The top aqueous phase was eluted and collected

in a sterile microcentrifuge tube. 1 µL RNase-free molecular grade glycogen (10901393001, Merck), and an equal amount ice-cold isopropanol was added. Samples were incubated on ice for 20 minutes to allow precipitation of RNA and centrifuged for 20 minutes at 15 000 g. The supernatant was discarded, and the pellet was washed twice in 75% ethanol, with 5-minute centrifuge spins. The pellet is allowed to dry and is resuspended in 20 µL DEPC-treated water. Quality and quantification of RNA following dissolution was assessed and concentration measured using a spectrophotometer (Nanodrop-8000, ND-8000-GL, ThermoFisher Scientific). Quantification of RNA targets was assessed by RT-qPCR. Synthesis of cDNA used the qScript cDNA synthesis kit (7331174, QuantaBio), 200 ng of RNA was added to the 1X master mix alongside 1X qScript reverse transcriptase and the final volume was adjusted to 20 µL with the addition of nuclease-free water. Samples were placed in a thermocycler for the following steps: 22ºC for 5 minutes, 42ºC for 1 hour, and 82ºC for 5 minutes. The product of cDNA synthesis was diluted 1:25 in nuclease-free water and proceeded with RT-qPCR quantification. The same reaction was prepared as for gDNA quantification, mentioned prior (primer concentration was 400 nM).

RNA-sequencing and analysis

Prior to sequencing, PolyA mRNA was enriched. RNA libraries were then prepared commercially by Novogene, and commercially assessed for quality. Sequencing of RNA was paired end of 150 bp in length and sequenced on Illumina NovaSeq platforms.

FASTQ files were trimmed using TRIMMOMATIC PE (v0.39) (Bolger *et al.*, 2014). Once trimmed, files were aligned to the *D. melanogaster* genome (BDGP6.56, FlyBase release FB2024_01), using HISAT2 (v2.2.1), after the construction of an HISAT2 index with the build function (Kim *et al*, 2019). SAMtools (v1.19.2) was used to convert the SAM files and to sort the BAM files based on genomic coordinates (Li *et al*, 2009). Read counts were extracted using HTSeq count function (v0.13.5)(Anders *et al*, 2015), and differential expression analysis was conducted using DESeq2 in R (Love *et al*, 2014). To examine gene sets, values were extracted, and plotted with gene lists curated on FlyBase for spermatogenesis (GO:0009283) and mitochondrion (GO:0005739).

Primer list

UPF1: F 5′-CCAGCATCACCAACGATCTG-3′, R 5′-AGTTGTTGCACATGACCACC-3
UPF2: F 5′-TCAAGGCCACCGAGAAGATT-3′, R 5′-AATGCACCAGAACAACACCC-3′

UPF3: F 5′-CTCCCTTCCAGTGCTTCCTT-3′, R 5′-GGAGGGGTGTAGACTTGACC-3′
RpL32: F: 5′-CTCCCTTCCAGTGCTTCCTT-3′, R: 5′-GGAGGGGTGTAGACTTGACC-3′
Cox1: F 5′-TCCTGATATAGCATTCCCACGA-3′, R 5′-CCACCATGAGCAATTCCAGC-3′
ND4: F 5′-GCTCATGTTGAAGCTCCAGT-3′, R 5′-AAGCCTTTAAATCAGTTTGACGT-3′
Cyt-b: F 5′-CACCTGCCCATATTCAACCAGAATG-3′, R 5′-CAACTGGTCGAGCTCCAATTCAAG-3′
16S lrRNA: F 5′-AGTCTAACCTGCCCACTGAA-3′, R 5′-TCCAACCATTCATTCCAGCC-3′
TFAM: F 5′-CCCAGATTACCACCGTCGAG-3′, R 5′-TTGTTGGTCCCGCTTGAACT-3′

Data availability

All RNA-seq datasets generated, and corresponding gene expression raw count data can be found on the gene expression omnibus (GEO) repository, accession number GSE266138.

Acknowledgments

We would like to thank Hansong Ma and Ason Chiang for insightful discussions. We would like to thank the following for fly lines provided for this study. Helen White-Cooper (University of Cardiff) for sending us *bamGAL4:VP16*, Alicia Hidalgo (University of Birmingham) for providing us the *MhcGAL4* line for adult muscle experiments, and Hansong Ma (University of Birmingham) for providing, *Dj-GFP*, *BAC-TFAM-GFP*, and the unpublished *ubi-mito-mCherry* line. The authors are also grateful to the staff of the Birmingham Advanced Light Microscopy (BALM) facilities, at the University of Birmingham. Also, the STED super-resolution microscopy of SATHI-Central Discovery Centre, and Confocal microscopy and advanced light microscopy (Interdisciplinary school of Life Sciences, Institute of Sciences, Banaras Hindu University, India) facilities. We would also like to thank the Biological Sciences Research Council [BBSRC BB/S017984/1, and The Midlands Integrative Biosciences (Doctoral) Training Partnership (MIBTP) studentship to HLD] for funding this research.

References

Altamura N, Groudinsky O, Dujardin G, Slonimski PP (1992) Nam7 nuclear gene encodes a novel member of a family of helicases with a Zn-ligand motif and is involved in mitochondrial functions in *Saccharomyces cerevisiae*. *Journal of Molecular Biology* 224: 575-587

Anders S, Pyl PT, Huber W (2015) HTSeq--a Python framework to work with high-throughput sequencing data. *Bioinformatics* 31: 166-169

Anderson MA, Jodoin JN, Lee E, Hales KG, Hays TS, Lee LA (2009) Asunder is a critical regulator of dynein-dynactin localization during Drosophila spermatogenesis. *Mol Biol Cell* 20: 2709-2721

Asher EB, Groudinsky O, Dujardin G, Altamura N, Kermorgant M, Slonimski PP (1989) Novel class of nuclear genes involved in both mRNA splicing and protein synthesis in Saccharomyces cerevisiae mitochondria. *Mol Gen Genet* 215: 517-528

Bader G, Enkler L, Araiso Y, Hemmerle M, Binko K, Baranowska E, De Craene JO, Ruer-Laventie J, Pieters J, Tribouillard-Tanvier D *et al* (2020) Assigning mitochondrial localization of dual localized proteins using a yeast Bi-Genomic Mitochondrial-Split-GFP. *Elife* 9

Bao JQ, Vitting-Seerup K, Waage J, Tang C, Ge Y, Porse BT, Yan W (2016) UPF2-Dependent Nonsense-Mediated mRNA Decay Pathway Is Essential for Spermatogenesis by Selectively Eliminating Longer 3′ UTR Transcripts. *PLoS genetics* 12

Bhattacharya A, Czaplinski K, Trifillis P, He F, Jacobson A, Peltz SW (2000) Characterization of the biochemical properties of the human Upf1 gene product that is involved in nonsense-mediated mRNA decay. *RNA* 6: 1226-1235

Bogenhagen DF (2012) Mitochondrial DNA nucleoid structure. *Bba-Gene Regul Mech* 1819: 914-920

Bolger AM, Lohse M, Usadel B (2014) Trimmomatic: a flexible trimmer for Illumina sequence data. *Bioinformatics* 30: 2114-2120

Brogna S, McLeod T, Petric M (2016) The Meaning of NMD: Translate or Perish. *Trends Genet* 32: 395-407

Brogna S, Wen J (2009) Nonsense-mediated mRNA decay (NMD) mechanisms. *Nat Struct Mol Biol* 16: 107-113

Brooks AN, Duff MO, May G, Yang L, Bolisetty M, Landolin J, Wan K, Sandler J, Booth BW, Celniker SE *et al* (2015) Regulation of alternative splicing in Drosophila by 56 RNA binding proteins. *Genome Res* 25: 1771-1780

Bykov YS, Flohr T, Boos F, Zung N, Herrmann JM, Schuldiner M (2022) Widespread use of unconventional targeting signals in mitochondrial ribosome proteins. *Embo Journal* 41

Chacinska A, Koehler CM, Milenkovic D, Lithgow T, Pfanner N (2009) Importing Mitochondrial Proteins: Machineries and Mechanisms. *Cell* 138: 628-644

Chakrabarti S, Jayachandran U, Bonneau F, Fiorini F, Basquin C, Domcke S, Le Hir H, Conti E (2011) Molecular mechanisms for the RNA-dependent ATPase activity of Upf1 and its regulation by Upf2. *Mol Cell* 41: 693-703

Chapin A, Hu H, Rynearson SG, Hollien J, Yandell M, Metzstein MM (2014) In vivo determination of direct targets of the nonsense-mediated decay pathway in Drosophila. *G3 (Bethesda)* 4: 485-496

Chen H, Ma J, Kong F, Song N, Wang C, Ma X (2022) UPF1 contributes to the maintenance of endometrial cancer stem cell phenotype by stabilizing LINC00963. *Cell Death Dis* 13: 257

Culbertson MR (1999) RNA surveillance - unforeseen consequences for gene expression, inherited genetic disorders and cancer. *Trends in Genetics* 15: 74-80

Czaplinski K, Weng Y, Hagan KW, Peltz SW (1995) Purification and characterization of the Upf1 protein - a factor involved in translation and messenger RNA degradation. *RNA* 1: 610-623

de Pinto B, Lippolis R, Castaldo R, Altamura N (2004) Overexpression of Upf1p compensates for mitochondrial splicing deficiency independently of its role in mRNA surveillance. *Mol Microbiol* 51: 1129-1142

De S, Edwards DM, Dwivedi V, Wang J, Varsally W, Dixon HL, Singh AK, Owuamalam PO, Wright MT, Summers RP *et al* (2022) Genome-wide chromosomal association of Upf1 is linked to Pol II transcription in Schizosaccharomyces pombe. *Nucleic Acids Res* 50: 350-367

DeLuca SZ, O'Farrell PH (2012) Barriers to male transmission of mitochondrial DNA in sperm development. *Dev Cell* 22: 660-668

Dorogova NV, Bolobolova EU, Akhmetova KA, Fedorova SA (2013) Drosophila male-sterile mutation emmenthal specifically affects the mitochondrial morphogenesis. *Protoplasma* 250: 515-520

Fabian L, Brill JA (2012) Drosophila spermiogenesis: Big things come from little packages. *Spermatogenesis* 2: 197-212

Fanourgakis G, Lesche M, Akpinar M, Dahl A, Jessberger R (2016) Chromatoid Body Protein TDRD6 Supports Long 3′ UTR Triggered Nonsense Mediated mRNA Decay. *PLoS genetics* 12

Fatscher T, Boehm V, Gehring NH (2015) Mechanism, factors, and physiological role of nonsense-mediated mRNA decay. *Cell Mol Life Sci* 72: 4523-4544

Fiorini F, Bagchi D, Le Hir H, Croquette V (2015) Human Upf1 is a highly processive RNA helicase and translocase with RNP remodelling activities. *Nature communications* 6: 7581

Fukasawa Y, Tsuji J, Fu SC, Tomii K, Horton P, Imai K (2015) MitoFates: Improved Prediction of Mitochondrial Targeting Sequences and Their Cleavage Sites. *Molecular & Cellular Proteomics* 14: 1113-1126

Giansanti MG, Fuller MT (2012) What Drosophila spermatocytes tell us about the mechanisms underlying cytokinesis. *Cytoskeleton (Hoboken)* 69: 869-881

Giansanti MG, Sechi S, Frappaolo A, Belloni G, Piergentili R (2012) Cytokinesis in Drosophila male meiosis. *Spermatogenesis* 2: 185-196

Goetz AE, Wilkinson M (2017) Stress and the nonsense-mediated RNA decay pathway. *Cell Mol Life Sci* 74: 3509-3531

Hales KG, Fuller MT (1997) Developmentally regulated mitochondrial fusion mediated by a conserved, novel, predicted GTPase. *Cell* 90: 121-129

Han X, Wei YL, Wang H, Wang FL, Ju ZY, Li TL (2018) Nonsense-mediated mRNA decay: a 'nonsense' pathway makes sense in stem cell biology. *Nucleic Acids Research* 46: 1038-1051

He F, Jacobson A (2015) Nonsense-Mediated mRNA Decay: Degradation of Defective Transcripts Is Only Part of the Story. *Annu Rev Genet*

Henderson KD, Andrew DJ (2000) Regulation and function of Scr, exd, and hth in the Drosophila salivary gland. *Dev Biol* 217: 362-374

Hogg JR, Goff SP (2010) Upf1 senses 3'UTR length to potentiate mRNA decay. *Cell* 143: 379-389

Holt IJ, Reyes A (2012) Human mitochondrial DNA replication. *Cold Spring Harb Perspect Biol* 4

Holzbaur EL, Hammarback JA, Paschal BM, Kravit NG, Pfister KK, Vallee RB (1991) Homology of a 150K cytoplasmic dynein-associated polypeptide with the Drosophila gene Glued. *Nature* 351: 579-583

Hug N, Longman D, Caceres JF (2016) Mechanism and regulation of the nonsense-mediated decay pathway. *Nucleic Acids Res* 44: 1483-1495

Hurt JA, Robertson AD, Burge CB (2013) Global analyses of UPF1 binding and function reveal expanded scope of nonsense-mediated mRNA decay. *Genome Res* 23: 1636-1650

Joers P, Jacobs HT (2013) Analysis of replication intermediates indicates that Drosophila melanogaster mitochondrial DNA replicates by a strand-coupled theta mechanism. *PLoS One* 8: e53249

Karousis ED, Nasif S, Muhlemann O (2016) Nonsense-mediated mRNA decay: novel mechanistic insights and biological impact. *Wiley Interdiscip Rev RNA* 7: 661-682

Kim D, Paggi JM, Park C, Bennett C, Salzberg SL (2019) Graph-based genome alignment and genotyping with HISAT2 and HISAT-genotype. *Nature biotechnology* 37: 907-915

Kim J, Kim HS, Chung JH (2023) Molecular mechanisms of mitochondrial DNA release and activation of the cGAS-STING pathway. *Exp Mol Med* 55: 510-519

Kim YK, Maquat LE (2019) UPFront and center in RNA decay: UPF1 in nonsense-mediated mRNA decay and beyond. *RNA* 25: 407-422

Lee HS, Simon JA, Lis JT (1988) Structure and Expression of Ubiquitin Genes of Drosophila-Melanogaster. *Molecular and Cellular Biology* 8: 4727-4735

Lee W, Zamudio-Ochoa A, Buchel G, Podlesniy P, Marti Gutierrez N, Puigros M, Calderon A, Tang HY, Li L, Mikhalchenko A *et al* (2023) Molecular basis for maternal inheritance of human mitochondrial DNA. *Nat Genet* 55: 1632-1639

Leeds P, Peltz SW, Jacobson A, Culbertson MR (1991) The product of the yeast Upf1 gene is required for rapid turnover of messenger RNAs containing a premature translational termination codon. *Genes & development* 5: 2303-2314

Lehtiniemi T, Bourgery M, Ma L, Ahmedani A, Mäkelä M, Asteljoki J, Olotu O, Laasanen S, Zhang FP, Tan K *et al* (2022) SMG6 localizes to the chromatoid body and shapes the male germ cell transcriptome to drive spermatogenesis. *Nucleic Acids Research* 50: 11470-11491

Lewis DL, Farr CL, Farquhar AL, Kaguni LS (1994) Sequence, Organization, and Evolution of the a+T Region of Drosophila-Melanogaster Mitochondrial-DNA. *Molecular Biology and Evolution* 11: 523-538

Li AYZ, Di Y, Rathore S, Chiang AC, Jezek J, Ma H (2023) Milton assembles large mitochondrial clusters, mitoballs, to sustain spermatogenesis. *Proc Natl Acad Sci U S A* 120: e2306073120

Li H, Handsaker B, Wysoker A, Fennell T, Ruan J, Homer N, Marth G, Abecasis G, Durbin R, Genome Project Data Processing S (2009) The Sequence Alignment/Map format and SAMtools. *Bioinformatics* 25: 2078-2079

Love MI, Huber W, Anders S (2014) Moderated estimation of fold change and dispersion for RNA-seq data with DESeq2. *Genome Biol* 15: 550

Lu KL, Yamashita YM (2017) Germ cell connectivity enhances cell death in response to DNA damage in the Drosophila testis. *Elife* 6

Lykke-Andersen S, Jensen TH (2015) Nonsense-mediated mRNA decay: an intricate machinery that shapes transcriptomes. *Nat Rev Mol Cell Biol* 16: 665-677

Moura M, Osswald M, Leca N, Barbosa J, Pereira AJ, Maiato H, Sunkel CE, Conde C (2017) Protein Phosphatase 1 inactivates Mps1 to ensure efficient Spindle Assembly Checkpoint silencing. *Elife* 6

Nechaev S, Fargo DC, dos Santos G, Liu LW, Gao Y, Adelman K (2010) Global Analysis of Short RNAs Reveals Widespread Promoter-Proximal Stalling and Arrest of Pol II in. *Science* 327: 335-338

Noguchi T, Koizumi M, Hayashi S (2011) Sustained elongation of sperm tail promoted by local remodeling of giant mitochondria in Drosophila. *Curr Biol* 21: 805-814

Patel MR (2017) Inheritance: Male mtDNA Just Can't Catch a Break. *Curr Biol* 27: R264-R266

Petric Howe M, Patani R (2023) Nonsense-mediated mRNA decay in neuronal physiology and neurodegeneration. *Trends Neurosci* 46: 879-892

Ramirez F, Dundar F, Diehl S, Gruning BA, Manke T (2014) deepTools: a flexible platform for exploring deep-sequencing data. *Nucleic Acids Res* 42: W187-191

Rehwinkel J, Letunic I, Raes J, Bork P, Izaurralde E (2005) Nonsense-mediated mRNA decay factors act in concert to regulate common mRNA targets. *RNA* 11: 1530-1544

Riley JS, Tait SW (2020) Mitochondrial DNA in inflammation and immunity. *EMBO reports* 21: e49799

Robinson JT, Thorvaldsdottir H, Turner D, Mesirov JP (2023) igv.js: an embeddable JavaScript implementation of the Integrative Genomics Viewer (IGV). *Bioinformatics* 39

Santel A, Winhauer T, Blumer N, Renkawitz-Pohl R (1997) The Drosophila don juan (dj) gene encodes a novel sperm specific protein component characterized by an unusual domain of a repetitive amino acid motif. *Mech Dev* 64: 19-30

Savojardo C, Bruciaferri N, Tartari G, Martelli PL, Casadio R (2020) DeepMito: accurate prediction of protein sub-mitochondrial localization using convolutional neural networks. *Bioinformatics* 36: 56-64

Schindelin J, Arganda-Carreras I, Frise E, Kaynig V, Longair M, Pietzsch T, Preibisch S, Rueden C, Saalfeld S, Schmid B *et al* (2012) Fiji: an open-source platform for biological-image analysis. *Nature methods* 9: 676-682

Schuster CM, Davis GW, Fetter RD, Goodman CS (1996) Genetic dissection of structural and functional components of synaptic plasticity. I. Fasciclin II controls synaptic stabilization and growth. *Neuron* 17: 641-654

Shami GJ, Samarska IV, Koek GH, Li A, Palma E, Chokshi S, Wisse E, Braet F (2023) Giant mitochondria in human liver disease. *Liver Int* 43: 2365-2378

Singh AK, Choudhury SR, De S, Zhang J, Kissane S, Dwivedi V, Ramanathan P, Orsini L, Hebenstreit D, Brogna S (2019) The RNA helicase UPF1 associates with mRNAs co-transcriptionally and is required for the release of mRNAs from transcription sites. *Elife* 2019;8:e41444

Singh AK, Lakhotia SC (2024) Visualizing dynamic organization of nuclei and mitochondria during spermatogenesis in Drosophila. In: *Experiments with Drosophila for Biology Courses*, Lakhotia S.C. (ed.)Indian Academy of Sciences Bengaluru:

Singh AK, Zhang J, Hebenstreit D, Brogna S (2020) Evidence of slightly increased Pol II pausing in UPF1-depleted Drosophila melanogaster cells. *MicroPubl Biol* 2020

Staszewski J, Lazarewicz N, Konczak J, Migdal I, Maciaszczyk-Dziubinska E (2023) UPF1-From mRNA Degradation to Human Disorders. *Cells* 12

Tenenbaum CM, Gavis ER (2016) Removal of Drosophila Muscle Tissue from Larval Fillets for Immunofluorescence Analysis of Sensory Neurons and Epidermal Cells. *J Vis Exp*

Torres TT, Dolezal M, Schlotterer C, Ottenwalder B (2009) Expression profiling of Drosophila mitochondrial genes via deep mRNA sequencing. *Nucleic Acids Res* 37: 7509-7518

Wang LJ, Hsu T, Lin HL, Fu CY (2021) Modulation of mitochondrial nucleoid structure during aging and by mtDNA content in Drosophila. *Biol Open* 10

White-Cooper H (2012) Tissue, cell type and stage-specific ectopic gene expression and RNAi induction in the Drosophila testis. *Spermatogenesis* 2: 11-22

Yu Z, O'Farrell PH, Yakubovich N, DeLuca SZ (2017) The Mitochondrial DNA Polymerase Promotes Elimination of Paternal Mitochondrial Genomes. *Curr Biol* 27: 1033-1039

Zaepfel BL, Zhang Z, Maulding K, Coyne AN, Cheng W, Hayes LR, Lloyd TE, Sun S, Rothstein JD (2021) UPF1 reduces C9orf72 HRE-induced neurotoxicity in the absence of nonsense-mediated decay dysfunction. *Cell Rep* 34: 108925

Zhang Y, Chen Y, Gucek M, Xu H (2016) The mitochondrial outer membrane protein MDI promotes local protein synthesis and mtDNA replication. *EMBO J* 35: 1045-1057

Zund D, Gruber AR, Zavolan M, Muhlemann O (2013) Translation-dependent displacement of UPF1 from coding sequences causes its enrichment in 3' UTRs. *Nat Struct Mol Biol* 20: 936-943

Zuniga G, Levy S, Ramirez P, De Mange J, Gonzalez E, Gamez M, Frost B (2023) Tau-induced deficits in nonsense-mediated mRNA decay contribute to neurodegeneration. *Alzheimers Dement* 19: 405-420

Figures and legends

Figure 1

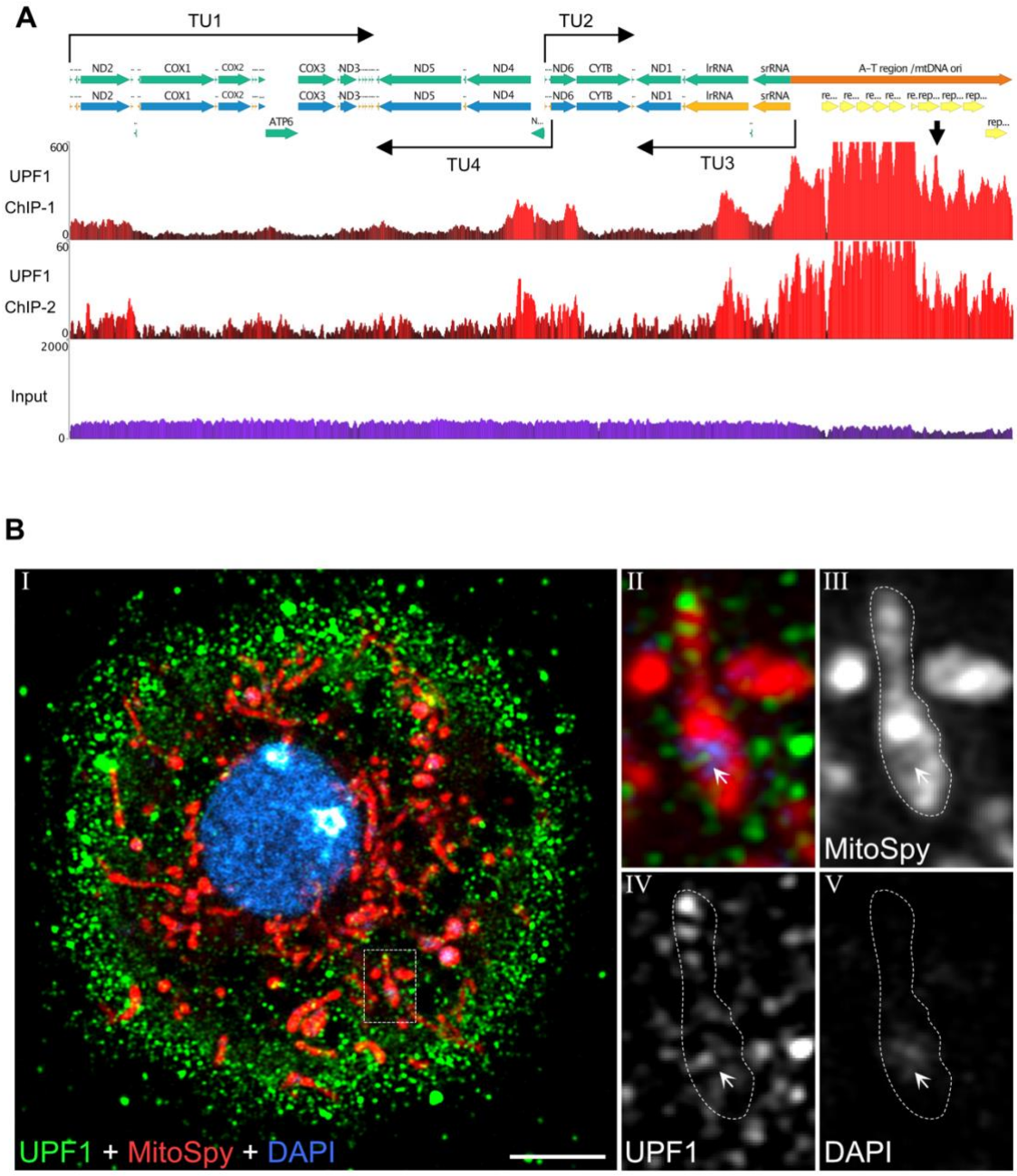

Figure 1. UPF1 mtDNA association and mitochondrial localisation in S2 cells. (**A**) The top schematic shows the linear map of the mtDNA and the location of the four transcription start sites and the corresponding transcription units (TUs), TU1 and TU2 on the top strand, TU3 and TU4 on the bottom strand. The protein-coding and rRNA genes are indicated in green, the A-T region / NCR is indicated in orange, blue indicates protein coding genes, orange indicates small and large rRNA, srRNA and lrRNA, respectively, yellow arrows indicate sequence repeats within NCR. The black arrow indicates a prominent peak of enrichment at one of the interrepeat regions. The bottom panel shows the genome browsers enrichment profiles of two independent UPF1 ChIP-Seq experiments (red) and, as control, the profile of the input chromatin DNA (purple). The Y axes were not scaled equally, although the two UPF1 samples show different absolute levels of enrichment, the pattern is very similar. (**B**) Fluorescence immunolocalisation of endogenous UPF1 (green; using anti-UPF1 monoclonal antibody 7B12. A similar pattern is detected using 1C13, see Material and Methods) in S2 cells. The red signal corresponds to MitoSpy, a fluorescent dye that localises to the mitochondrial matrix (Materials and Methods). The blue signal corresponds to DAPI, which labels the nuclear DNA and the mtDNA. Panel I shows a merge image in the three channels of a whole cell: magnified views of the boxed region as shown in panels II – V, either as a merged image (panel II) or individual labelled channels in grey. The arrow points to a strong UPF1 signal dot adjacent to the DAPI stained region of the mitochondria. The images were taken using a Zeiss LSM900 confocal microscope equipped with a 63X objective lens (Materials and Methods). The scale bar corresponds to 10 µm.

Figure S1

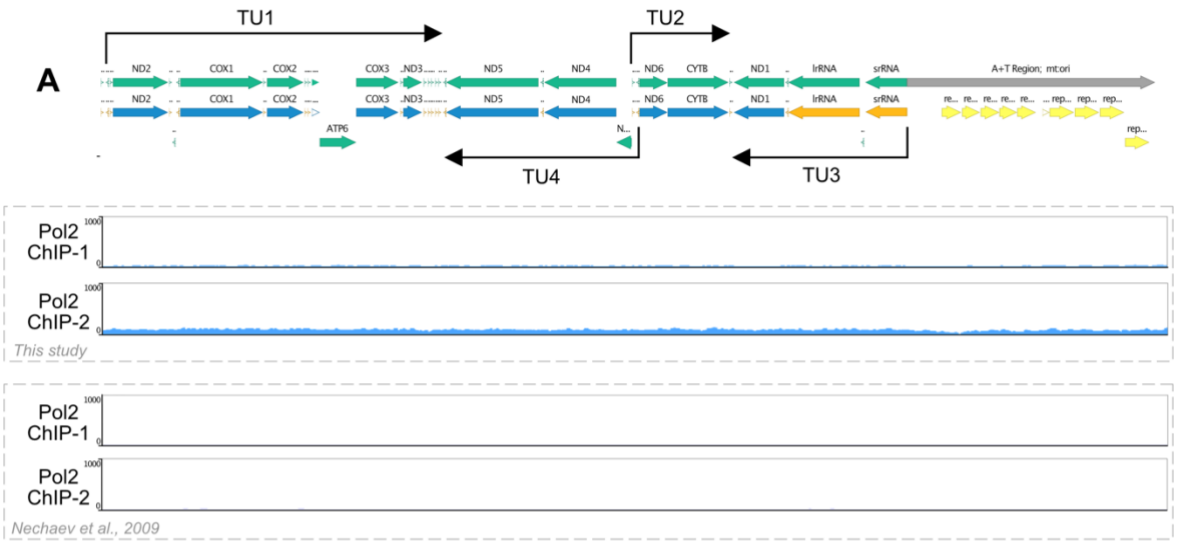
A
TU1
TU2
TU3
TU4
ND2
COX1
COX2
COX3
ND3
ND5
ND4
ND6
CYTB
ND1
lrRNA
srRNA
A+T Region; mt:ori
ATP6
Pol2 ChIP-1
Pol2 ChIP-2
This study
Nechaev et al., 2009

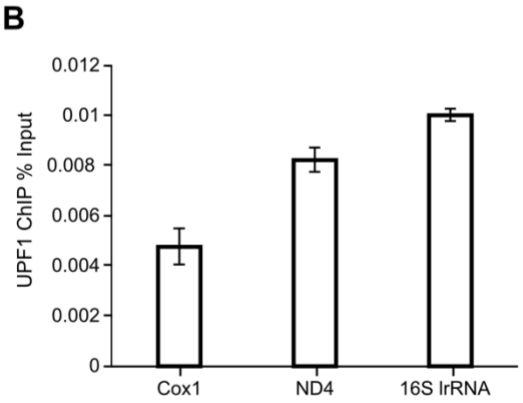
B
UPF1 ChIP % Input
0.012
0.01
0.008
0.006
0.004
0.002
0
Cox1
ND4
16S lrRNA

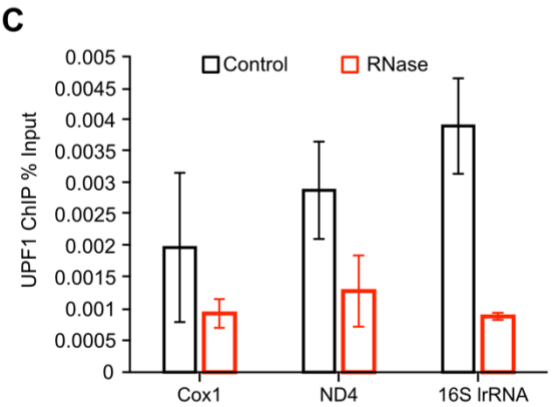
C
Control
RNase
UPF1 ChIP % Input
0.005
0.0045
0.004
0.0035
0.003
0.0025
0.002
0.0015
0.001
0.0005
0
Cox1
ND4
16S lrRNA

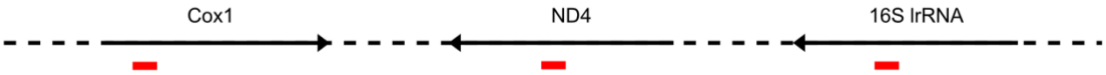
Cox1
ND4
16S lrRNA

Figure S1. UPF1 ChIP-qPCR validation and RNase sensitivity evidence. (**A**) Top panel shows the annotated linear map of the mitochondrial genome. First two panels below show lack of mtDNA enrichment in two independent Pol II ChIP-Seq experiments (Singh et al., 2020). The next two rows show lack of enrichment in two Pol II ChIP-Seq datasets from a different laboratory (Nechaev et al., 2010). (**B**) ChIP-qPCR examination of UPF1 association with the three mtDNA gene regions indicated, Cox1, ND4 and lrRNA. The location of the three primer pairs are indicated in red in the schematic below. (**C**) UPF1 ChIP-qPCR of the three mtDNA genes with, or without RNase treatment of the chromatin prior the IP (Material and Methods), error bars represent the standard error of the mean (SEM). The values are based on two separate ChIP experiments.

Figure S2

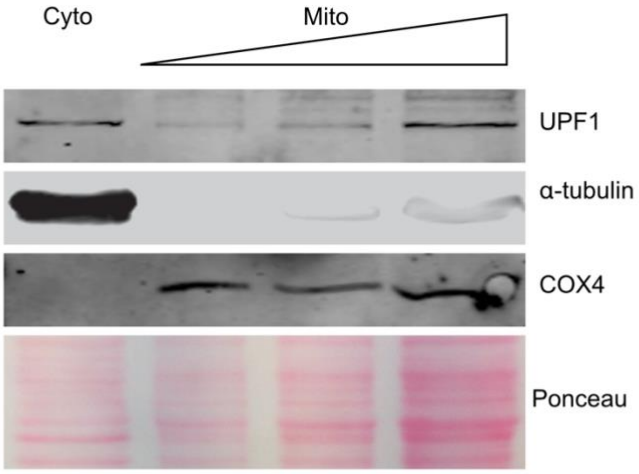

Figure S2. UPF1 copurifies with COX4 in S2 cells. Co-fractionation western blot experiment of cytoplasmic (Cyto) and mitochondrial (Mito) fractions. Both fractions were stained for UPF1 alongside α-tubulin and COX4 as controls for the cytoplasm and mitochondria, respectively. Ponceau staining of the membrane serves as a loading control.

Figure S3

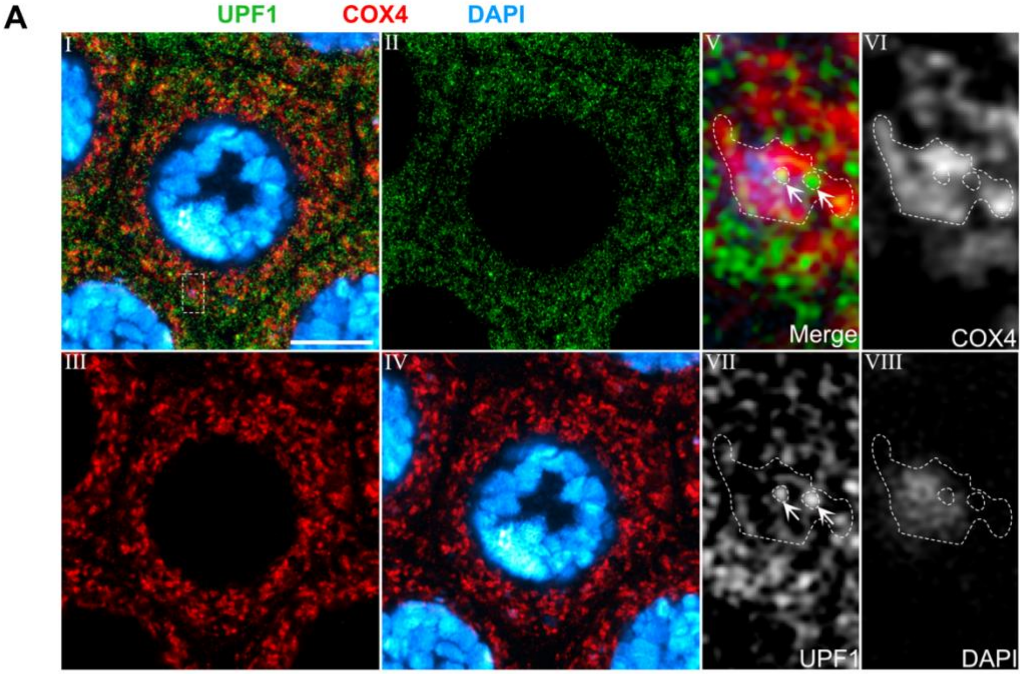

2nd Instar Larvae

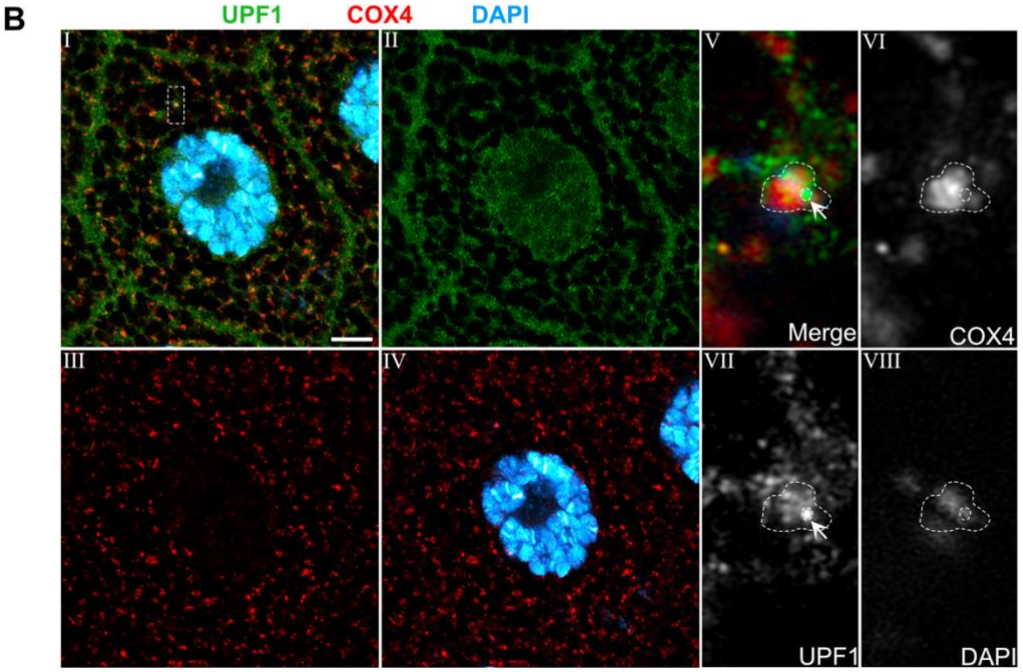

3rd Instar Larvae

Figure S3. Endogenous UPF1 colocalises with COX4 in salivary glands. Fluorescence immunolocalisation of endogenous UPF1 (green) and COX4 (red) as the mitochondrial marker. DAPI (blue) represents DNA (both nuclear and mtDNA). (**A**) Shows a second instar larva salivary gland cell. (**B**) A third instar larvae cell. In both instances, panel I represents a merged image of all three channels, UPF1 (panel II), COX4 (panel III). Panel IV represents both COX4 and DAPI. The boxed region is shown magnified in panels V-VIII, as merged (V) and grey panels for COX4 (VI), UPF1 (VII) and DAPI (VIII). Arrows point to foci of UPF1 adjacent to DAPI-stained regions of the mitochondria. Scale bar represents 10 µm.

Figure S4

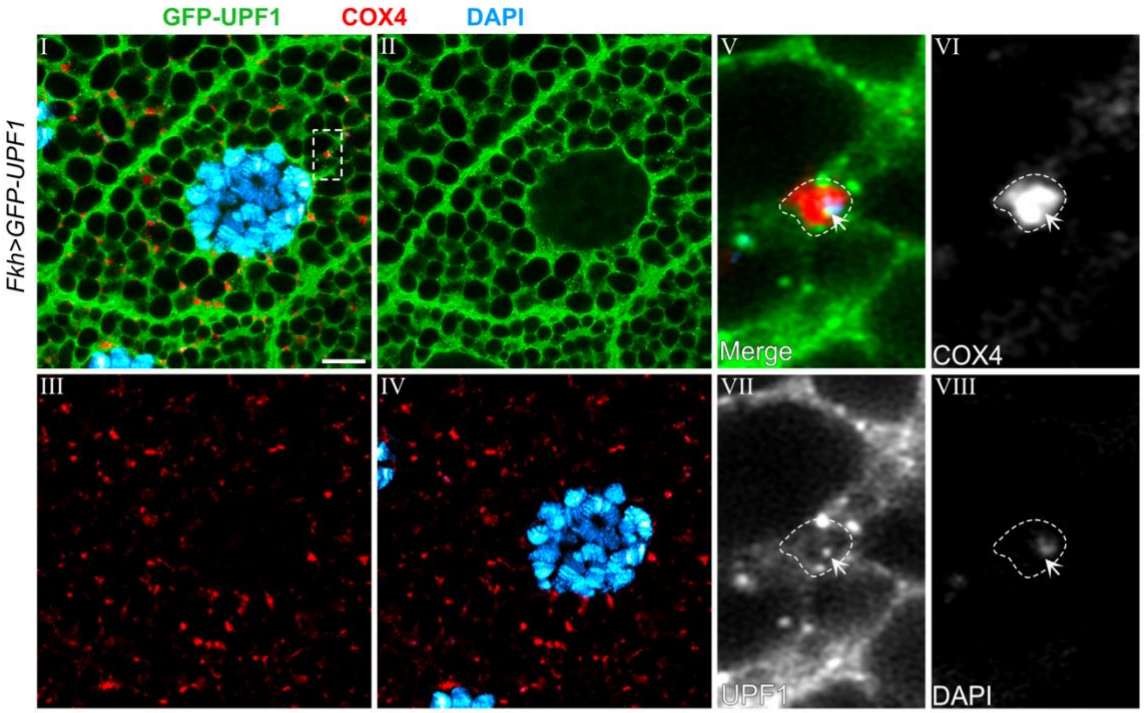
GFP-UPF1
COX4
DAPI
Fkh>GFP-UPF1
I
II
V
VI
Merge
COX4
III
IV
VII
VIII
UPF1
DAPI

Figure S4. A portion of GFP-tagged UPF1 localises to mitochondria in salivary glands. Fluorescence immunolocalisation of *FkhGAL4* driven expression of GFP-UPF1 (green) and immunostaining of endogenous COX4 (red). DAPI (blue) represents nuclear and mtDNA in third instar salivary glands. Panel I shows a merged image of all three channels, UPF1 (panel II), COX4 (panel III). Panel IV displays both COX4 and DAPI. The boxed region shown in panel I is magnified in panels V-VIII, as a merged image (V) and grey for COX4 (VI), UPF1 (VII) and DAPI (VIII). Arrows point to foci of UPF1 adjacent to DAPI-stained regions of the mitochondria. Scale bar represents 10 µm.

Figure 2

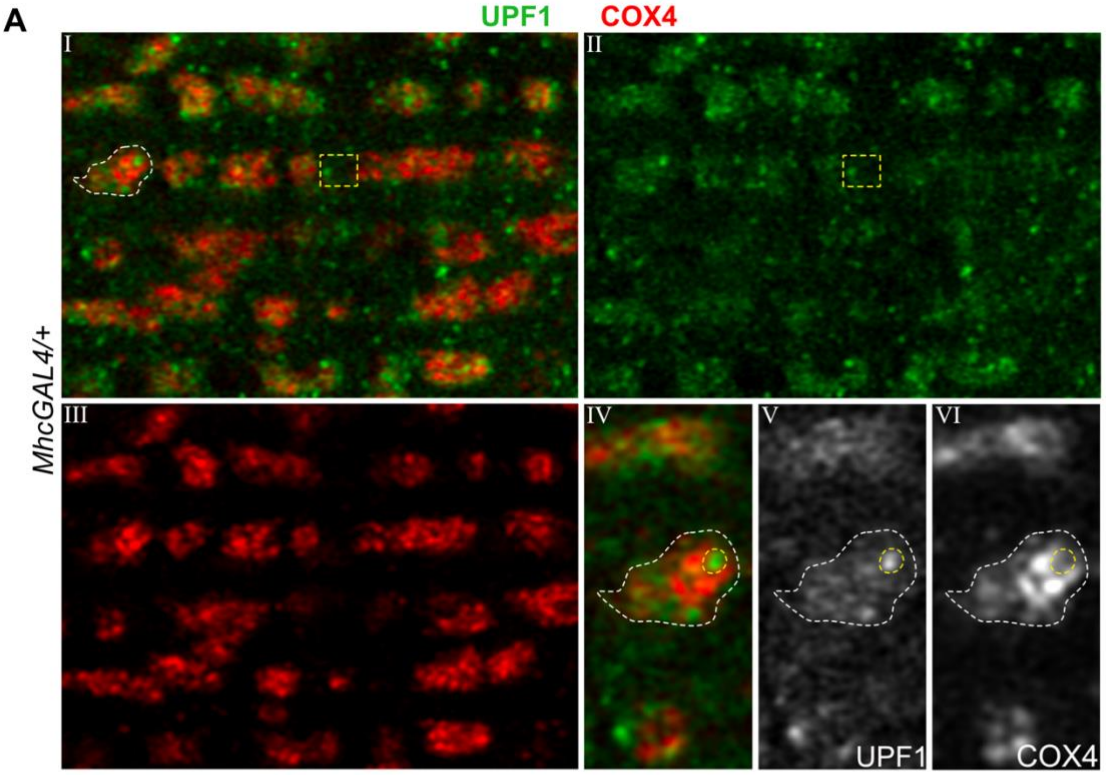
A
UPF1
COX4
I
II
MhcGAL4/+
III
IV
V
VI
UPF1
COX4

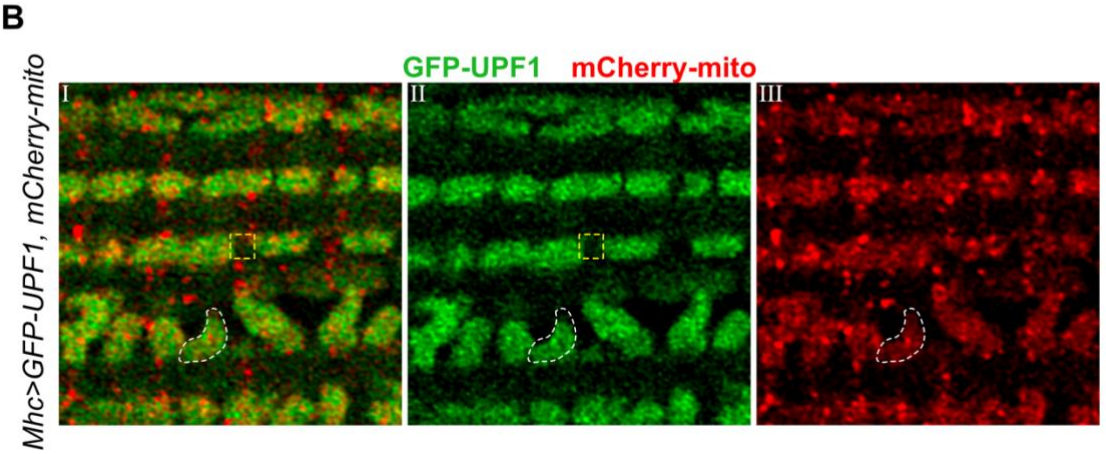
B
GFP-UPF1
mCherry-mito
Mhc>GFP-UPF1, mCherry-mito
I
II
III

Figure 2. UPF1 displays prominent mitochondrial localisation in flight muscles. (**A**) Fluorescence immunolocalisation of endogenous UPF1 (green) and COX4 (red) as the mitochondrial marker in indirect flight muscles. Panel I shows a merged image of both channels, UPF1 (panel II) and COX4 (panel III), with an example cytoplasmic region indicated by the yellow dashed rectangle. Panels IV-VI represent a magnified view of the mitochondrial region outlined in panel I, as the merged image (panel IV), or as individual channels in grey, UPF1 (panel V) and COX4 (panel VI). A strong dot of UPF1 signal is circled in yellow in the magnified views; this is localising in a region lacking COX4 signal. (**B**) Fluorescence localisation of *MhcGAL4* driven expression of GFP-UPF1 (green) and mCherry-mito (red) in indirect flight muscles. Panel I represents a merged image of both channels, GFP-UPF1 (panel II) and mCherry-mito (panel III), a cytoplasmic region is indicated by the yellow dashed rectangle.

Figure 3

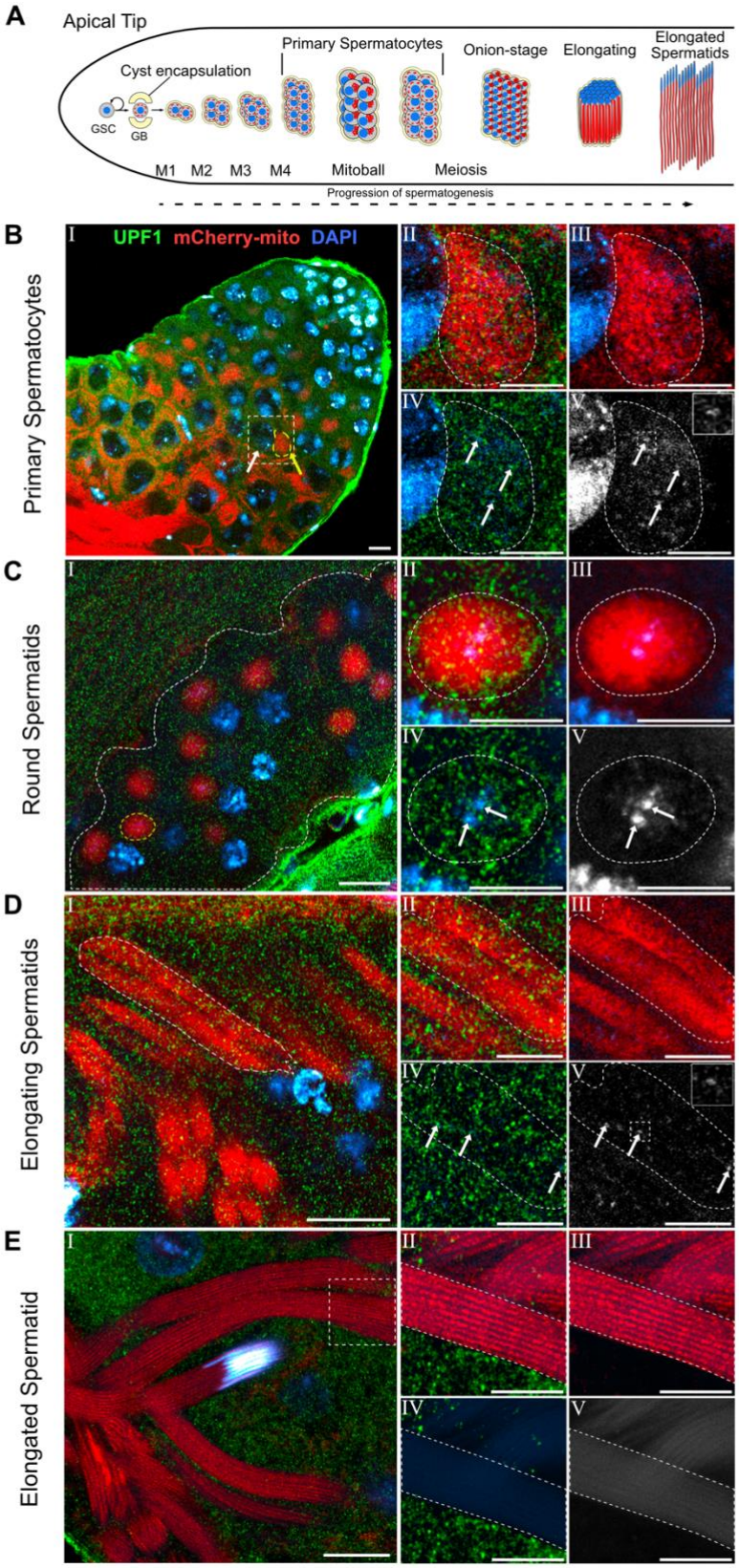
A
Apical Tip
Cyst encapsulation
GSC
GB
Primary Spermatocytes
Onion-stage
Elongating
Elongated Spermatids
M1
M2
M3
M4
Mitoball
Meiosis
Progression of spermatogenesis
B
Primary Spermatocytes
UPF1 mCherry-mito DAPI
C
Round Spermatids
D
Elongating Spermatids
E
Elongated Spermatid

Figure 3 UPF1 mitochondrial localisation during spermatogenesis. (**A**) Schematic of *Drosophila* spermatogenesis. A germinal stem cell (GSC) at the apical tip of the testes proliferates into a differentiating gonialblast (GB), and a self-renewing GSC. The GB is enclosed by within a cyst made of two cyst cells and undergoes four rounds of mitosis (M1-M4) to produce 16 diploid primary spermatocytes. The mitochondria (red) cluster to form the Mitoball, a transient structure adjacent to the nucleus (blue). The mitoball disperses and the primary spermatocytes undergo meiosis to produce 64 haploid, round onion-stage spermatids, the mitochondria have fused to form the nebenkern adjacent to the nucleus. Each spermatid then undergoes elongation, with the unfurling of the nebenkern into the major and minor mitochondrial derivatives, and into the elongating tail. (**B-E**) Fluorescent immunolocalisation of endogenous UPF1 (green), imaging of ubiquitously expressed mCherry-mito (red) as the mitochondrial marker, and DAPI (blue) to stain nuclear and mitochondria DNA. (**B**) Primary spermatocytes. Panel I shows a merged image of the three channels, with a primary spermatocyte outlined with the white dotted box, the white arrow corresponds to the nucleus and the yellow arrow marks the Mitoball. Panel II represents the merged magnified view of the outlined primary spermatocyte in panel I, the Mitoball is outlined in white. Panel III – IV represent mCherry-mito (panel III) and UPF1 (panel IV) together with DAPI. Panel V shows DAPI alone, with a magnified inset showing one nucleoid indicated by the topmost arrow (top right). White arrows in panels IV and V indicate UPF1 dots proximal to DAPI signal. (**C**) Shows a cyst with round-stage spermatids. Magnified views of the nebenkern outlined in yellow in panel I, are indicated in panels II-V. White arrows in panels IV and V point to two clusters of mtDNA/nucleoids in the centre nebenkern. (**D**) Localisation in elongating spermatids. Magnified view of a portion of the area (major and minor mitochondrial derivatives) outlined by the dashed line in panel I are shown in panels II – V. Arrows in panels IV and V show dots of UPF1 adjacent to DAPI, magnification inset of DAPI is seen in panel V (top right). Panel V shows DAPI alone. Arrows in panels IV and V indicate UPF1 dots proximal to residual DAPI foci. (**E**) Imaging of elongated spermatids, which show absence of UPF1. Panel I shows the outlined region which is magnified in panels II-V which show absence of UPF1 and DAPI foci in the spermatid tail, panels IV-V. Scale bars in B-E, panel I represent 10 µm, scale bars in B-E, panels II-IV represent 5 µm.

Figure S5

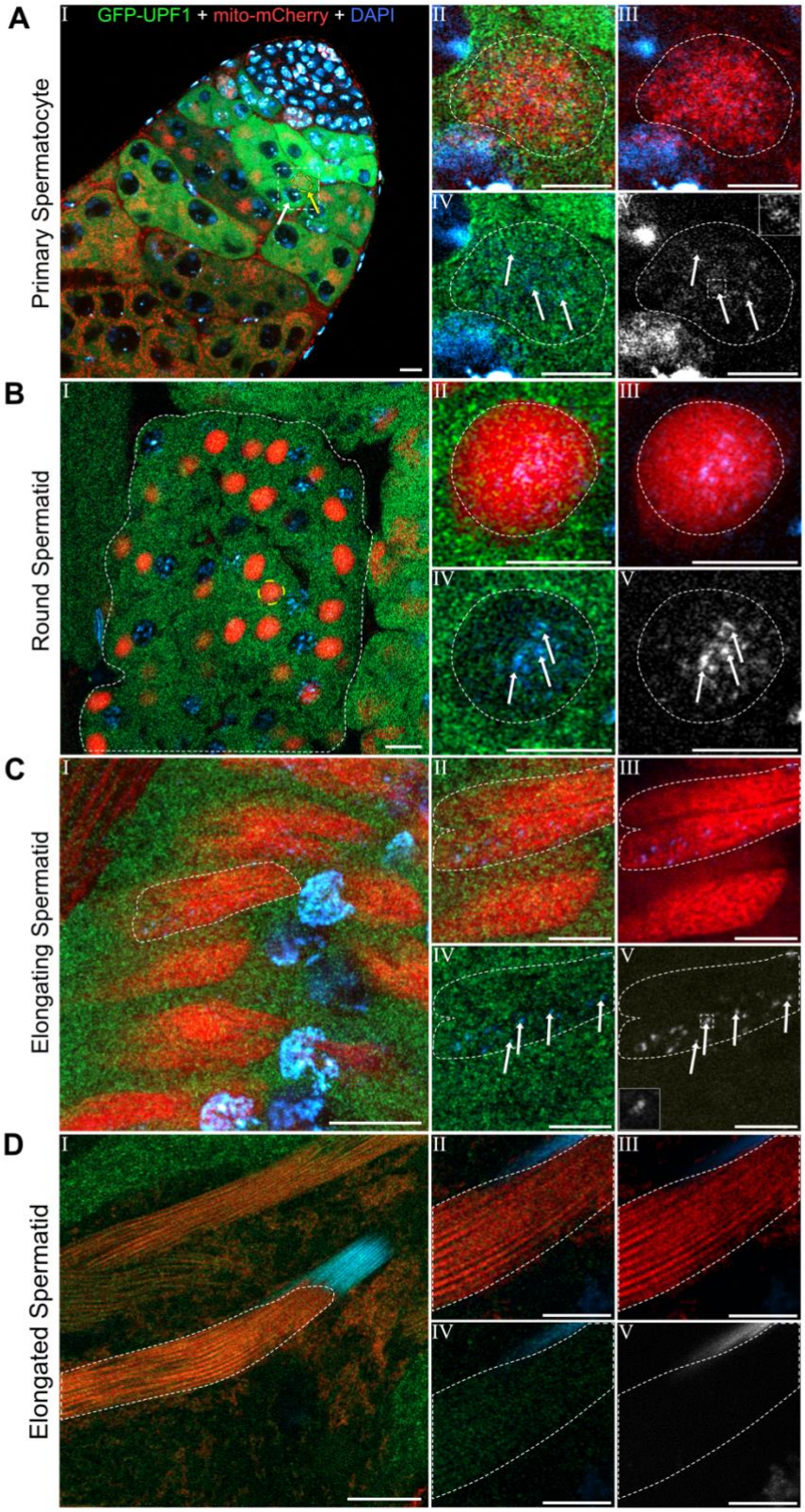
A
Primary Spermatocyte
I
GFP-UPF1 + mito-mCherry + DAPI
II
III
IV
V
B
Round Spermatid
I
II
III
IV
V
C
Elongating Spermatid
I
II
III
IV
V
D
Elongated Spermatid
I
II
III
IV
V

Figure S5. GFP-UPF1 also localises to mitochondria in developing spermatids. Fluorescent localization of GFP-UPF1 (green), ubiquitously expressed mCherry-mito (red) as the mitochondrial marker, and DAPI (blue) to stain nuclear and mitochondria DNA. (**A**) Primary spermatocytes. Panel I shows a merged image of the three channels, with a primary spermatocyte outlined by the white dotted box, the white arrow corresponds to the nucleus and the yellow arrow marks the Mitoball. Panel II represents the merged magnified view of the outlined primary spermatocyte in panel I, the mitoball is outlined by the dashed white line. Panel III – IV represent mCherry-mito (panel III) and GFP-UPF1 (panel IV) together with DAPI. Panel V shows DAPI alone, with a magnified inset panel showing an example of a nucleoid region (top right). Arrows in panels IV and V indicate strong UPF1 signals proximal to DAPI signals. (**B**) Shows a cyst with round-stage spermatids. Magnified views of the nebenkern outlined in yellow in panel I are shown in panels II-V. White arrows in panels IV and V indicate GFP-UPF1 dots adjacent to DAPI in the centre nebenkern. (**C**) GFP-UPF1 localisation in elongating spermatids. Magnified view of a portion of the area (major and minor mitochondrial derivatives) outlined by the dashed line in panel I are shown in panels II – V. Arrows in panels IV and V show strong signals of GFP-UPF1 adjacent to DAPI, magnification inset of DAPI is seen in panel V (bottom left). Panel V shows DAPI alone. Arrows in panels IV and V indicate strong GFP-UPF1 signals proximal to DAPI signal. (**D**) Imaging of elongated spermatids, which show absence of GFP-UPF1. Panel I shows the outlined region which is magnified in panels II-V which show absence of GFP-UPF1 and DAPI foci in the spermatid tail, panels IV-V. Scale bars in B-E, panel I represent 10 µm, scale bars in B-E, panels II-IV represent 5 µm.

Figure 4

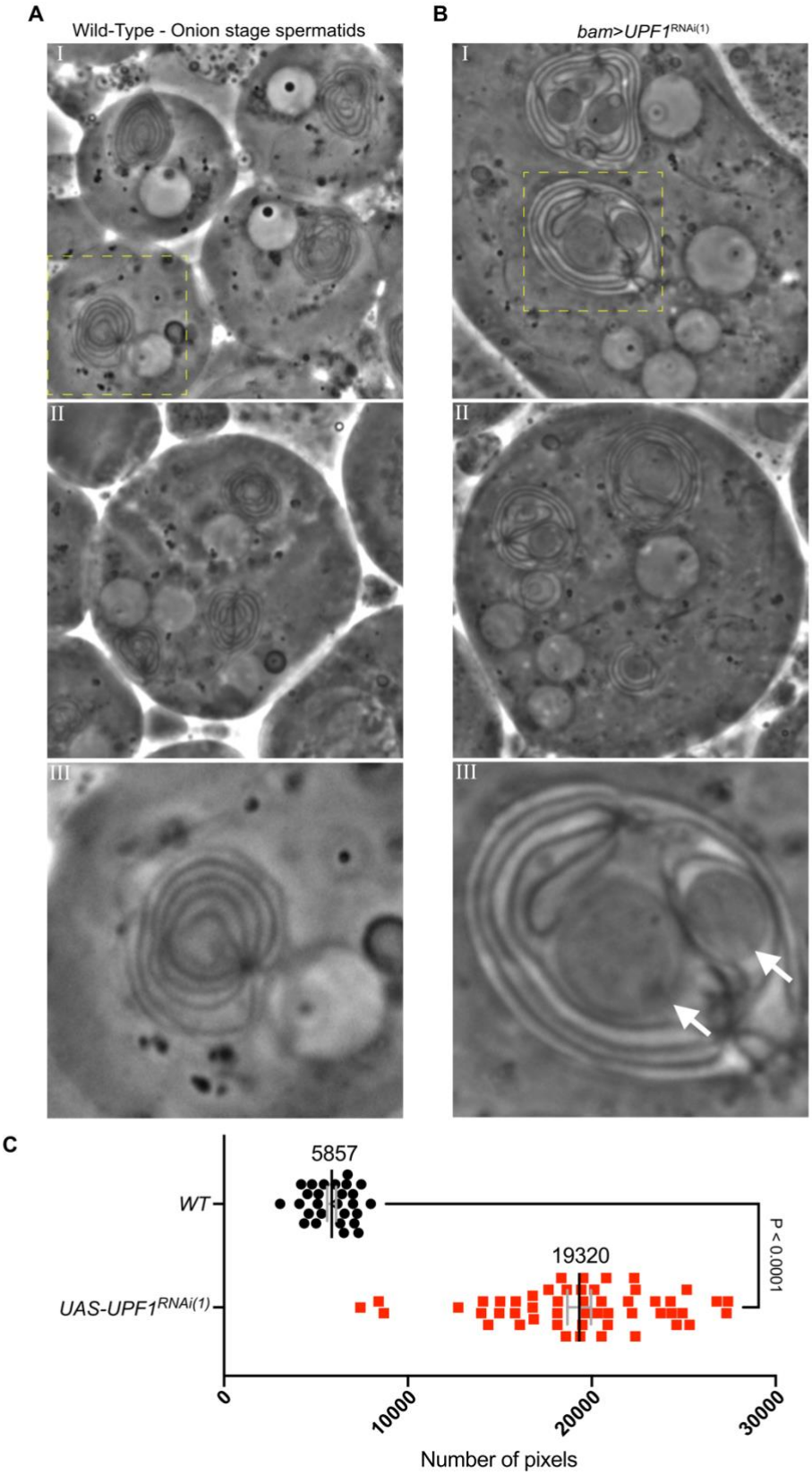
A
Wild-Type - Onion stage spermatids
B
bam>UPF1RNAi(1)
I
II
III
C
5857
WT
19320
UAS-UPF1RNAi(1)
P < 0.0001
0
10000
20000
30000
Number of pixels

Figure 4. Depletion of UPF1 in developing spermatids results in meiotic defects and abnormal nebenkern formation. (**A-B**) Phase contrast microscopy of round stage spermatids. (**A**) WT round stage spermatids. Panel I shows four distinct round spermatids. Panel II shows a syncytium-like structure containing four nuclei, each with an adjacent nebenkern. The magnified view of the yellow outlined region in panel I is shown in panel III below. (**B**) Round spermatids following *bamGAL4* driven $UPF1^{RNAi(1)}$. Panel I shows syncytium-like structure corresponding to several round stage spermatids, with nuclei of differing sizes and large nebenkern. Panel II shows a cyst of round stage spermatids, with a syncytium appearance. The magnified view of the abnormal nebenkern outlined in yellow in panel I is shown in panel III. Arrows in panel III indicate large spheroid bodies within the nebenkern. (**C**) Quantification of nebenkern area (number of pixels) in WT and UPF1 depleted testes. Error bars represent the SEM. Statistical significance was calculated using a two-tailed unpaired t-test. RNAi efficiency was estimated by RT-qPCR using UPF1-specific primers. RNA was reduced to 30-40 % of control.

Figure S6

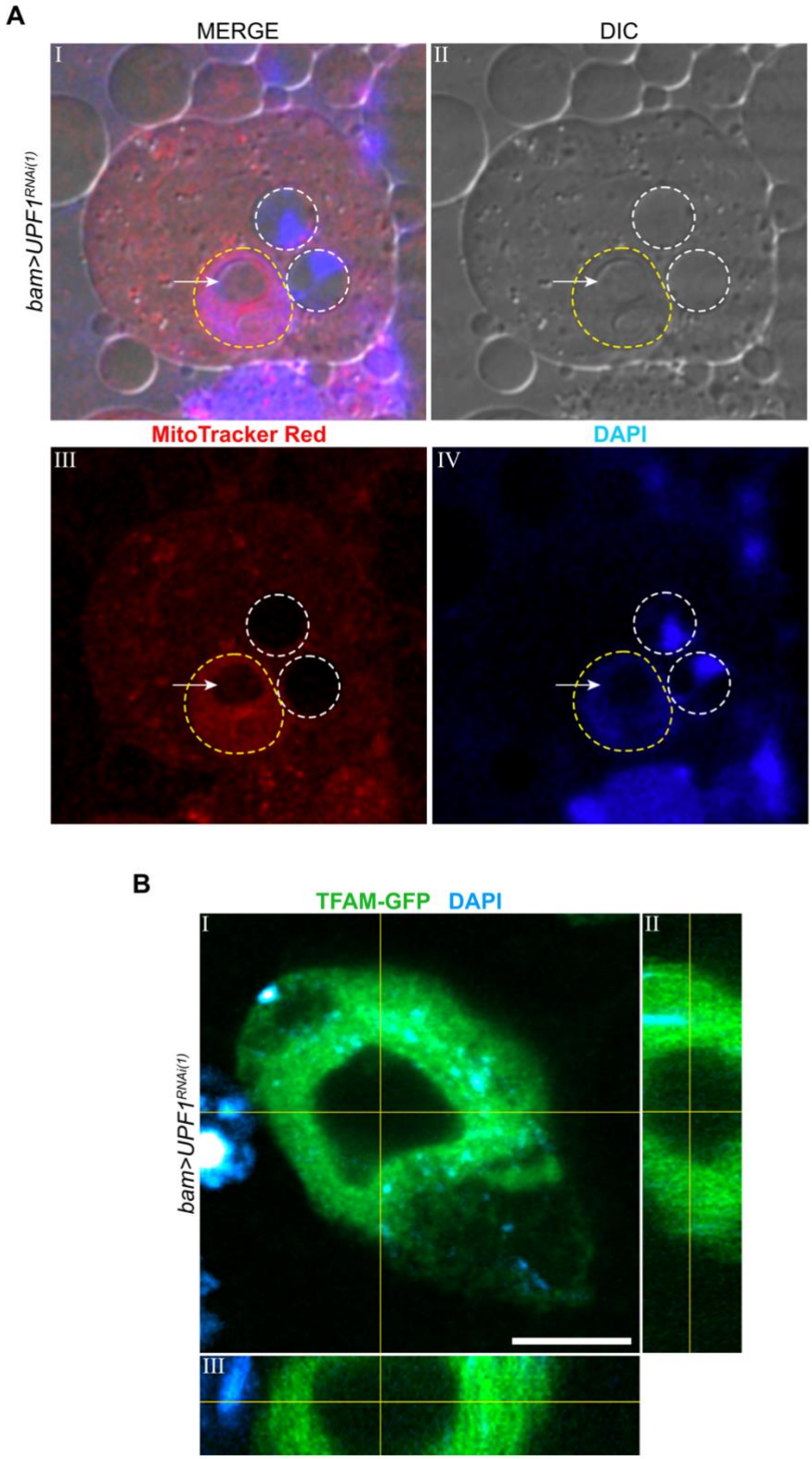
A
MERGE
DIC
I
II
bam>UPF1RNAi(1)
MitoTracker Red
DAPI
III
IV
B
TFAM-GFP DAPI
I
II
III
bam>UPF1RNAi(1)

Figure S6. The abnormal spheroid bodies present within the UPF1KD nebenkern do not stain for DAPI. (**A**) DIC and fluorescent microscopy of round stage spermatid syncytium in *bam>UPF1*$^{RNAi(1)}$ testes, with MitoTracker Red CMXROS (red) as the mitochondrial marker, and DAPI (blue) to mark nuclear and mitochondrial DNA . Panel I represents the merged image of all channels, DIC (panel II), MitoTracker Red (panel III) and DAPI (panel IV). The nebenkern is outlined in yellow, whilst two adjacent nuclei are outlined in white. The spheroid bodies in the nebenkern are circled by dashed lines and one, yellow, indicated by the white arrow. The structure within the nebenkern does not stain with either MitoTracker Red (panel III) or DAPI (panel IV). (**B**) DAPI visualisation of mtDNA in *bamGAL4* driven *UPF1*$^{RNAi(1)}$. The nebenkern is marked by the expression TFAM-GFP (green) and contains mtDNA (blue), in the area not occupied by the spheroid body. Panel I is the central optical section of the nebenkern morphology, panel II and III show the orthogonal views of the region in the YZ and XZ planes, respectively.

Figure S7

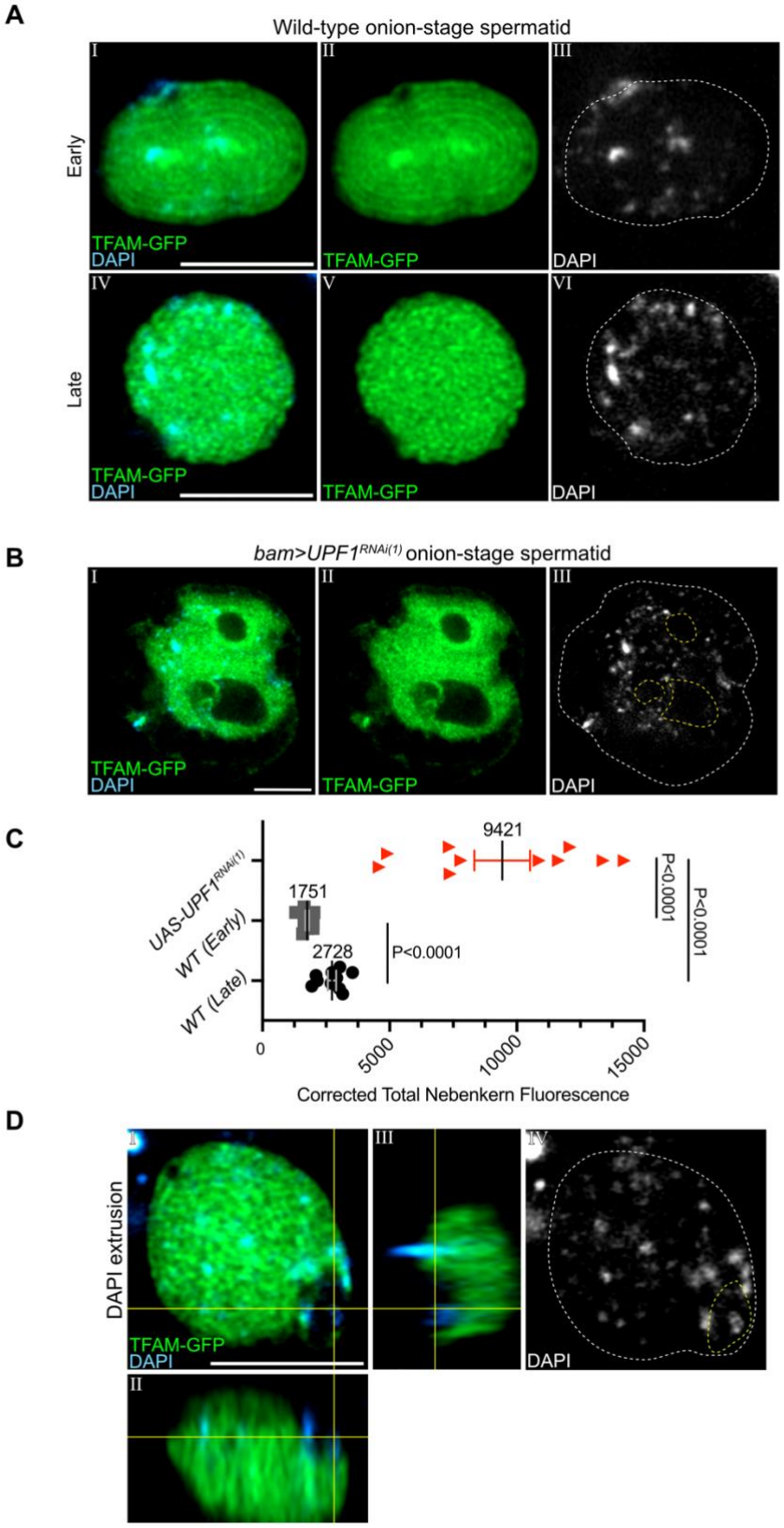
A
Wild-type onion-stage spermatid
Early
Late
I
II
III
IV
V
VI
TFAM-GFP
DAPI
B
bam>UPF1RNAi(1) onion-stage spermatid
C
UAS-UPF1RNAi(1)
WT (Early)
WT (Late)
1751
2728
9421
P<0.0001
P<0.0001
P<0.0001
0
5000
10000
15000
Corrected Total Nebenkern Fluorescence
D
DAPI extrusion

Figure S7. DNA-containing protrusions are formed at the nebenkern periphery in wild type but not in UPF1KD spermatids. Imaging of nebenkern in WT, and UPF1KD testes, using TFAM-GFP as the mitochondrial marker (green) and DAPI to stain DNA (blue). Scale bars all represent 5 µm. (**A**) WT early (panels I-III), and late (panels IV-VI) nebenkern morphology. Panels I and IV represent a merged image of the two channels, panels II, and V show TFAM-GFP, mtDNA is shown alone in grey in panels III and IV with the nebenkern outlined in white. (**B**) Nebenkern morphology in UPF1KD testes (panels I-III). Panel I shows a merged image of both channels. Panel II shows TFAM-GFP alone. Panel III shows mtDNA alone in grey with the nebenkern outlined in white, and vacuole-like bodies outlined in yellow. (**C**) Total corrected fluorescence quantification of mtDNA in the nebenkern in WT and UPF1KD testes. mtDNA was quantified for both stages of nebenkern seen in WT testes. Error bars represent the SEM. significance was calculated by using a two-tailed unpaired t-test. (**D**) WT nebenkern with vesicular-like structures at its periphery. Panel I shows a merged image of both channels, TFAM-GFP and DAPI. Panel II and III represent the orthogonal view of the XY and ZY planes, respectively. Panel IV shows DAPI alone in grey with the nebenkern and vesicular-like structure outlined in white and yellow, respectively.

Figure 5

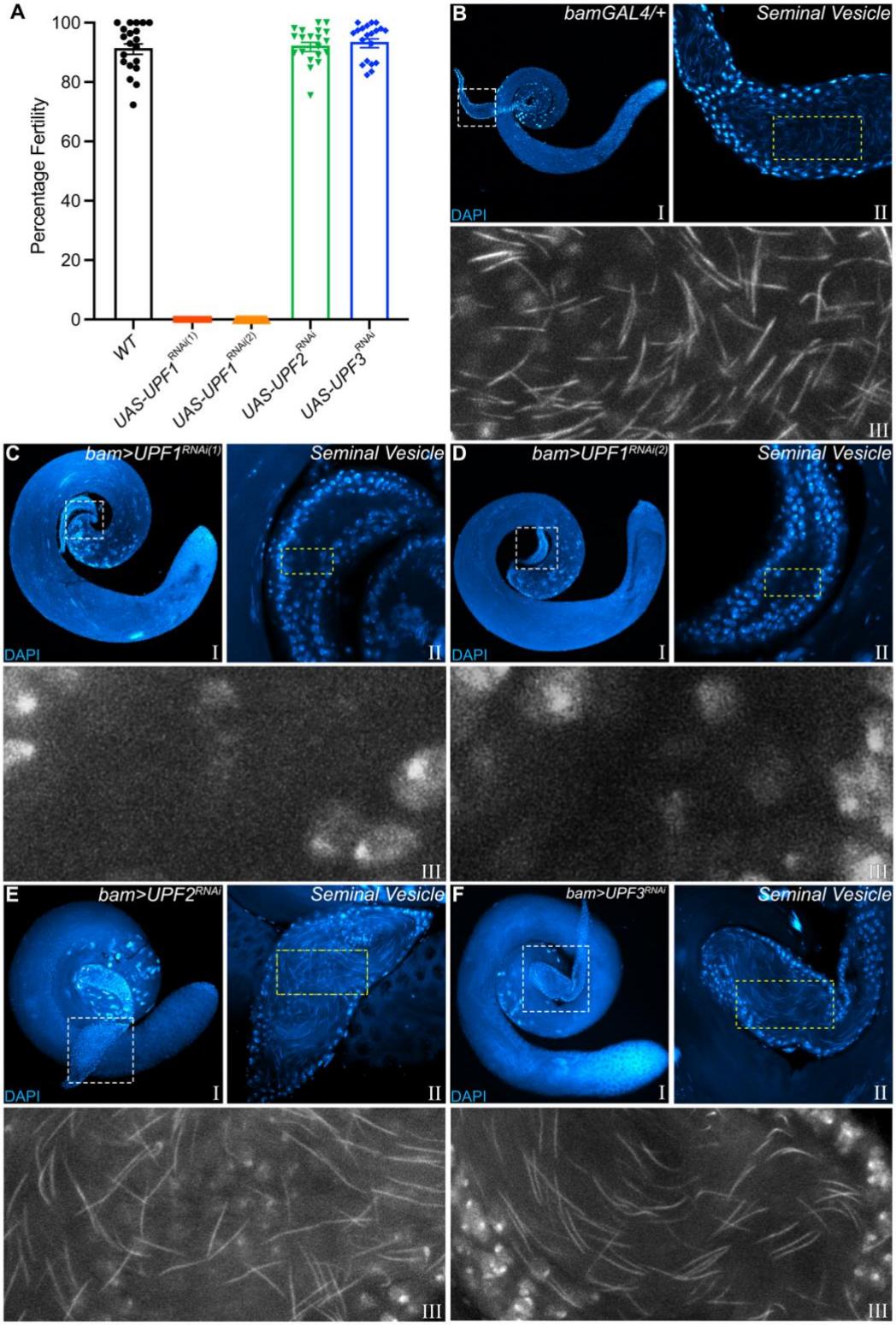
A
Percentage Fertility
100
80
60
40
20
0
WT
UAS-UPF1 RNAi(1)
UAS-UPF1 RNAi(2)
UAS-UPF2 RNAi
UAS-UPF3 RNAi
B
bamGAL4/+
Seminal Vesicle
DAPI
I
II
III
C
bam>UPF1 RNAi(1)
Seminal Vesicle
DAPI
I
II
III
D
bam>UPF1 RNAi(2)
Seminal Vesicle
DAPI
I
II
III
E
bam>UPF2 RNAi
Seminal Vesicle
DAPI
I
II
III
F
bam>UPF3 RNAi
Seminal Vesicle
DAPI
I
II
III

Figure 5. Depletion of UPF1, but not of other NMD factors causes male sterility. (**A**) Fertility scoring of males depleted of UPF1, UPF2 and UPF3 in testes crossed with wild type females. Percentage fertility calculated by: (number of pupa ÷ number of eclosed flies) ÷ number of eggs laid. (**B-F**) Confocal images of DAPI-stained testes, to mark nuclear DNA. (**B**) WT testes (*bamGAL4:vp16)*, panel I. Panel II shows the seminal vesicle indicated in panel I by the white box. Panel III shows the magnified inset of the yellow box in panel II in grey, this is the content of the seminal vesicle with visible spermatid heads stained with DAPI (grey). (**C**) UPF1KD testes (*bam>UPF1*$^{RNAi(1)}$), panel I, show empty seminal vesicles (panel II) with no visible spermatids heads (panel III). (**D**) An empty seminal vesicle is seen again in a second line of UPF1KD (*bam>UPF1*$^{RNAi(2)}$; panels I-III). (**E**) UPF2KD testes (bam>*UPF2*^{RNAi}), panel I, demonstrate full seminal vesicles, with visible mature spermatid heads (panel II-III). (**F**) UPF3KD testes (*bam>UPF3*^{RNAi}), panel I, also shows mature spermatids in the seminal vesicle (panel II-III).

Figure S8

A

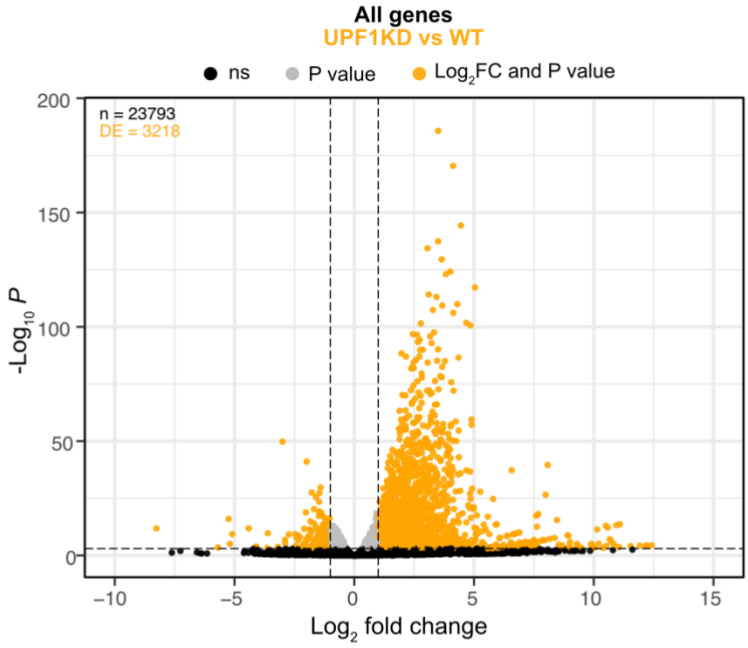

B

Top 10 upregulated

Gene Name	*Log_2 fold change*	*P.adj*
Mst57Da	12.4215665	1.72E-04
Acp53C14a	12.2003453	2.39E-04
Acp53Ea	12.1974041	3.11E-04
Acp76A	12.1764587	2.80E-04
Mst57Db	11.9166976	2.75E-04
CG43147	11.6140285	9.37E-03
BG642163	11.5393533	3.74E-04
lncRNA:CR43451	11.0881633	4.26E-13
CG9029	11.0625427	1.06E-03
Or49b	10.9401234	9.83E-13

Top 10 downregulated

Gene Name	*Log_2 fold change*	*P.adj*
lncRNA:CR45464	-8.26253133	2.25E-11
CG16826	-7.26011952	2.88E-02
SdicC	-5.69569207	1.45E-03
CG43902	-5.24711402	2.14E-15
whe	-5.19527950	5.57E-05
Cpr66Cb	-5.09685324	5.54E-09
1360{}6337	-4.57858613	3.02E-02
HB{}227	-4.40563406	2.16E-11
CG4678	-4.28273608	2.06E-02
l{}Sirt6-iso-1b	-4.22152041	5.67E-03

Figure S8. Approximately 14% of genes are mis-regulated in UPF1KD testes. DESeq2 differential expression analysis of all genes (n = 23798) in UPF1KD versus WT testes RNA-seq datasets. (**A**) Volcano plot of all differentially expressed genes (DEG; n = 3218; 2689 upregulated, 529 downregulated), significantly DEG (-1< LFC >1, P<0.05,) are shown in orange, those in grey indicate significant (P<0.05), but not highly misregulated (1> LFC >-1) and, those in black are non-significant (P>0.05). (**B**) Top misregulated genes for both upregulated (left panel) and downregulated (right panel), LFC and the P adjusted value (P.adj) is shown.

Figure 6

A

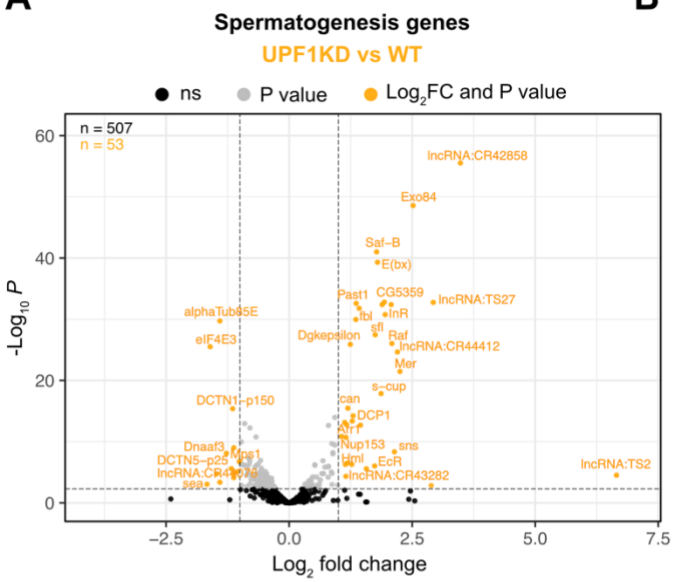

B

Top misregulated

Gene Name	*Log_2 fold change*	*P.adj*
lncRNA:TS2	6.65159341	1.73E-04
lncRNA:CR42858	3.47992322	4.56E-54
lncRNA:TS27	2.92864798	8.62E-32
lncRNA:TS26	2.88616385	1.55E-02
Exo84	2.51817483	2.87E-47
zfh2	2.46452525	1.66E-02
Mer	2.25169168	9.96E-21
lncRNA:CR44412	2.20001642	7.61E-24
sns	2.13869912	4.92E-08
Raf	2.08803110	3.36E-25
sea	-1.66874409	3.54E-03
eIF4E3	-1.60394871	1.09E-24
asun	-1.47227088	1.11E-04
alphaTub85E	-1.40713231	7.95E-29
lncRNA:CR44076	-1.40668490	1.82E-03
PCNA	-1.27476810	8.41E-08
lncRNA:CR44344	-1.17428456	1.85E-05
DCTN1-p150	-1.14732813	8.22E-15
MED20	-1.12576035	1.00E-04
Hp1e	-1.12520965	3.93E-04

C

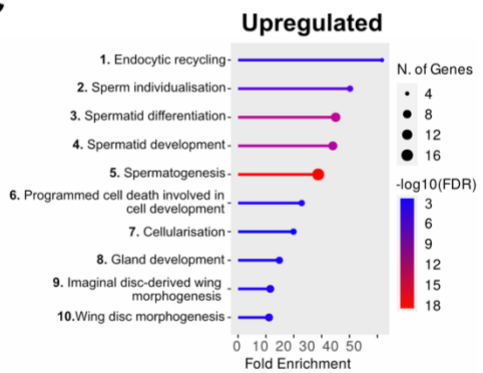

Pathway	*Genes*
1	*Past1, scat,* ***Mer, Exo84***
2	*EcR, Past1, scat,* ***Mer****, Dark*
3	*E(bx), EcR, scat, can, Past1,* ***sns, Mer****, Dark,* ***Exo84****, mfr*
4	*EcR, scat, can, Past1,* ***sns, Mer****, Dark,* ***Exo84****, mfr*
5	*E(bx), EcR, scat, can, Past1,* ***sns, Mer****, Dark,* ***Exo84****, mfr, Rcd-1, Eip74EF, fbl,* ***Raf****, sfl, ERR, InR*
6	*EcR, Eip74EF,* ***Mer****, Dark, N*
7	*EcR, Past1, scat,* ***Mer****, Dark*
8	*EcR, Eip74EF,* ***Raf****, N, Dark, InR*
9	*EcR, Past1,* ***Raf, zfh2****, N, fbl, sfl*
10	*EcR, Past1,* ***Raf, zfh2****, N, fbl, sfl*

D

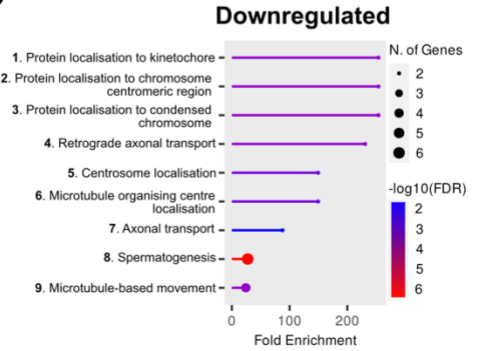

Pathway	*Genes*
1	*Mps1,* ***DCTN1-p150***
2	*Mps1,* ***DCTN1-p150***
3	*Mps1,* ***DCTN1-p150***
4	*DCTN5-p25,* ***DCTN1-p150***
5	***asun, DCTN1-p150***
6	***asun, DCTN1-p150***
7	*DCTN5-p25,* ***DCTN1-p150***
8	***asun****, Mps1, CG17669,* ***HP1e****, DCTN5-p25, eIF4E3*
9	***asun, DCTN1-p150,*** *CG17669, DCTN5-p25*

Figure 6. UPF1KD during spermatogenesis results in reduced expression of chromosomal segregation genes, and upregulation of genes required in spermatid differentiation. DESeq2 differential expression analysis of spermatogenesis genes (n = 507) in UPF1KD (averaged from both *bam>UPF1*$^{RNAi(1)}$ and *bam>UPF1*$^{RNAi(2)}$) versus WT testes RNA-seq samples. Values were calculated based on comparison against 23798 genes. (**A**) Volcano plot of DEG (n = 53; 40 upregulated, 13 downregulated), significantly DEG (-1< LFC >1, P<0.05) are shown in orange, those in grey indicate significant (P<0.05), but not highly misregulated (1> LFC >-1) and, those in black are non-significant (P>0.05). (**B**) Top 10 misregulated genes, both upregulated (top panel) and downregulated (bottom panel), LFC and the P.adj is shown. (**C-D**) Gene Ontology (GO) analysis of upregulated (**C**) and downregulated genes (**D**). Graph showing enriched GO terms (left panel), the node size is determined by number of genes associated with the given GO term, colour corresponds to the -$\log_{10}$(FDR), from blue (lowest) to red (highest), only pathways where an FDR of <0.05 are shown. The different GO terms are ordered based on fold enrichment value. Pathways are numbered numerically, and misregulated genes involved in these pathways, are shown in the corresponding table (right panel), with genes identified as highly misregulated amongst all genes shown in bold. Upregulated GO terms are numbered as following: GO:0001673 (1), GO:0043073 (2), GO:0030139 (3), GO:0034399 (4), GO:0000932 (5), GO:0031985 (6), GO:0005912 (7), GO:0016324 (8), GO:0090575 (9), and GO:0005911 (10). Downregulated GO terms are numbered: GO:0034501 (1), GO:0071459 (2), GO:1903083 (3), GO:0008090 (4), GO:0051642 (5), GO:0061842 (6), GO:0098930 (7), GO:0007283 (8), and GO:0007018 (9).

Figure S9

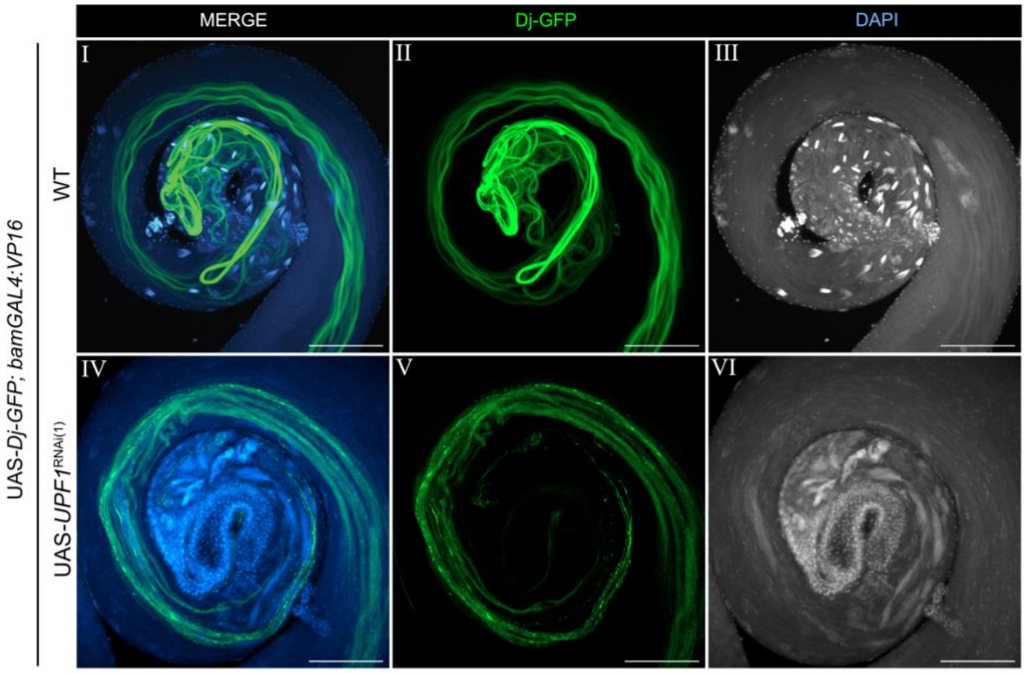
MERGE
Dj-GFP
DAPI
I
II
III
IV
V
VI
WT
UAS-UPF1RNAi(1)
UAS-Dj-GFP; bamGAL4:VP16

Figure S9. Fully elongated spermatids incorporating don juan (Dj) are produced in UPF1KD testes. Confocal microscopy of *bamGAL4* driven expression of *Dj*-GFP (green) and staining of DAPI to mark DNA (blue). WT testes (panel I) shows a merged image of both channels, with *Dj*-GFP marking the elongated spermatid tails (panel II) and DAPI marking the nuclei (panel III). Merged image of UPF1KD testes (*bam>UPF1*$^{RNAi(1)}$; panel IV), *Dj*-GFP and DAPI are shown separately (panel V and VI, respectively). Scale bar represents 100 µm.

Figure 7

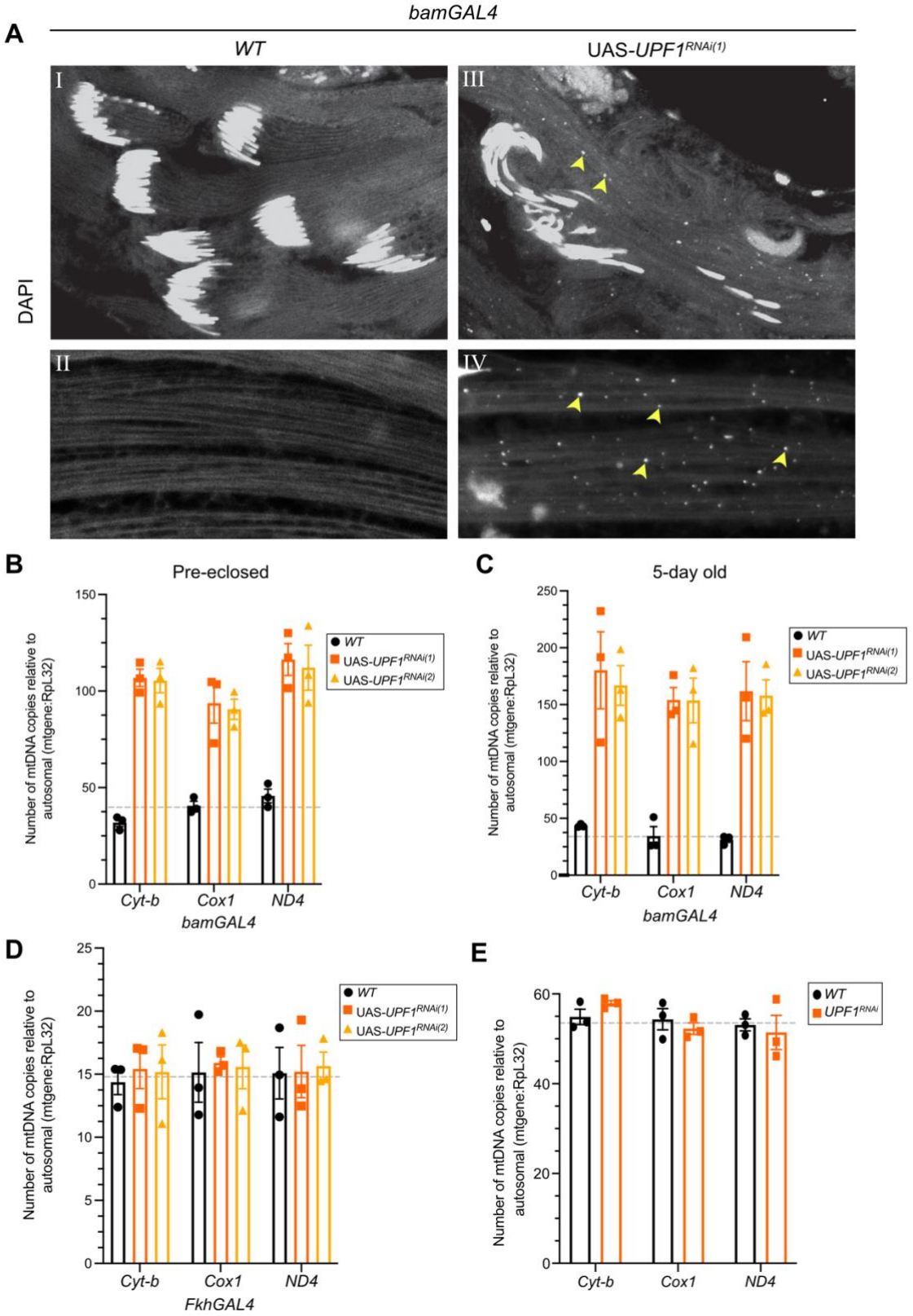
A
bamGAL4
WT
UAS-UPF1RNAi(1)
DAPI
I
II
III
IV
B
Pre-eclosed
Number of mtDNA copies relative to autosomal (mtgene:RpL32)
WT
UAS-UPF1RNAi(1)
UAS-UPF1RNAi(2)
Cyt-b
Cox1
ND4
bamGAL4
C
5-day old
D
FkhGAL4
E
UPF1RNAi

Figure 7. The elongated UPF1KD spermatids retain their mtDNA. (**A**) DAPI-stained elongated spermatid bundles in WT (panels I-II) and *UPF1*$^{RNAi(1)}$ (panels III-IV) testes. Panels II and IV represent magnified view of bundles of elongated spermatid tails. In panel III and IV DAPI signals represent putative mtDNA/nucleotides, examples are indicated by yellow arrows. (**B-E**) RT-qPCR of total genomic DNA (gDNA), using three mitochondrial genome loci: *Cyt-b*, *Cox1* and *ND4*, and normalised against the autosomal locus, *RpL32*, to calculate a ratio of mtDNA copy number. (**B**) In WT and UPF1KD testes from pre-eclosed, (**C**) 5-day old testes, (**D**) salivary glands and (**E**) S2 cells. Two *UPF1*^{RNAi} lines were driven in testes (**B** & **C,** red (*UPF1*$^{RNAi(1)}$) and blue bars (*UPF1*$^{RNAi(2)}$), respectively) and salivary glands (**D**) using *bamGAL4* and *FkhGAL4*. dsRNA was transfected into S2 cells to induce UPF1^{RNAi} (**E**). Error bars represent SEM, significance was calculated by using an unpaired t-test whereby $P \leq 0.05$.

Figure S10

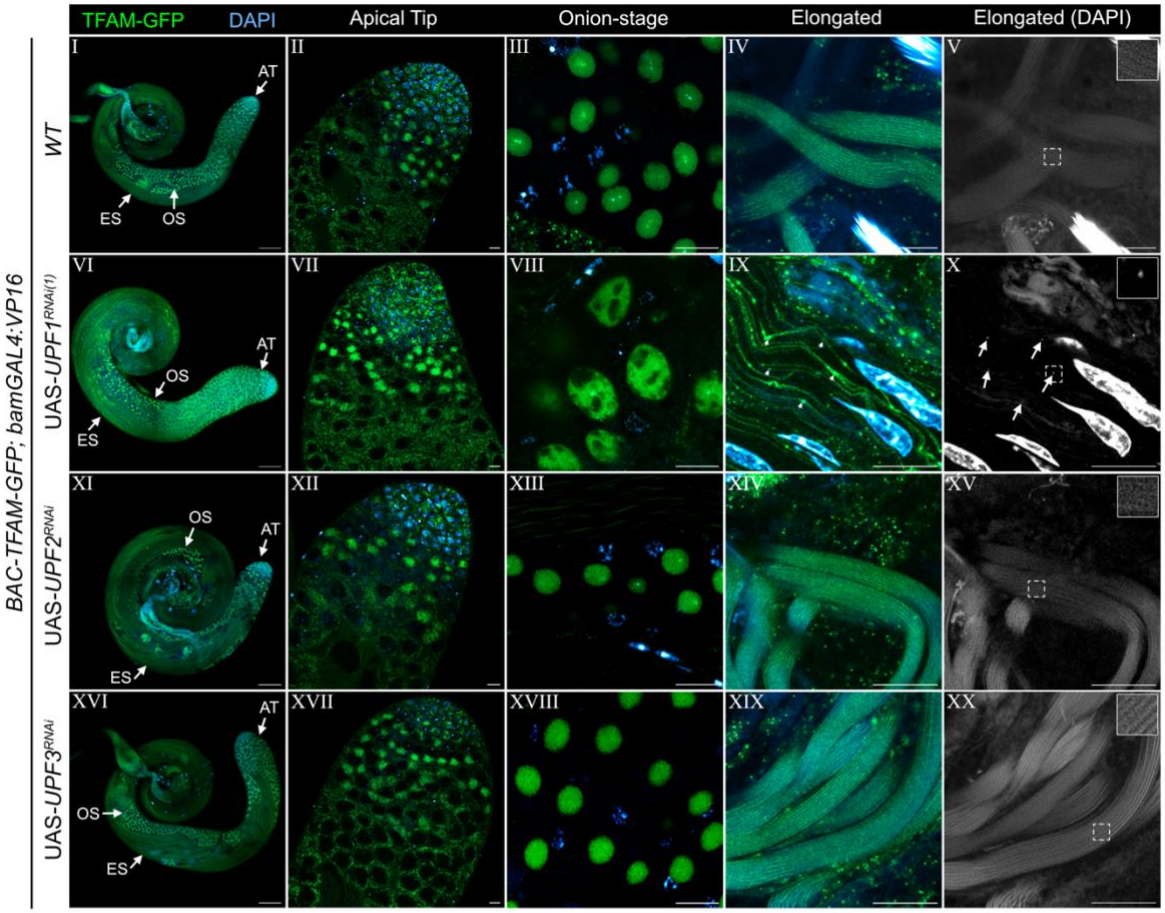
TFAM-GFP
DAPI
Apical Tip
Onion-stage
Elongated
Elongated (DAPI)
BAC-TFAM-GFP; bamGAL4:VP16
WT
UAS-UPF1RNAi(1)
UAS-UPF2RNAi
UAS-UPF3RNAi
I
II
III
IV
V
VI
VII
VIII
IX
X
XI
XII
XIII
XIV
XV
XVI
XVII
XVIII
XIX
XX
AT
ES
OS

Figure S10. DAPI signals co-localising with TFAM-GFP are observed in UPF1KD spermatid tails. Fluorescence visualisation of TFAM-GFP in wild type (panels I-IV) and UPF1 (panels VI-X), UPF2 (panels XI-XV) and UPF3 (panels XVI-XX) depleted testes. TFAM-GFP serves as a mitochondrial marker and mtDNA/nucleoids (green), tissues were also stained with DAPI to mark nuclear and mitochondrial DNA (blue). Merged views of whole testes (panels I, VI, XI and XVI; white arrows indicates the apical tip (AT), onion-stage spermatids (OS) and elongated spermatid (ES) tails. Magnified views of the apical tip of the testes (panels II, VII, XII, and XVII), onion-stage spermatids (panels III, VIII, XIII, and XVIII) and elongated spermatids (IV, IX, XIV and XIX) are shown. DAPI alone is shown for elongated spermatids (panels V, X, XV and XX). Scale bar represents 10 µm.

Figure 8

A

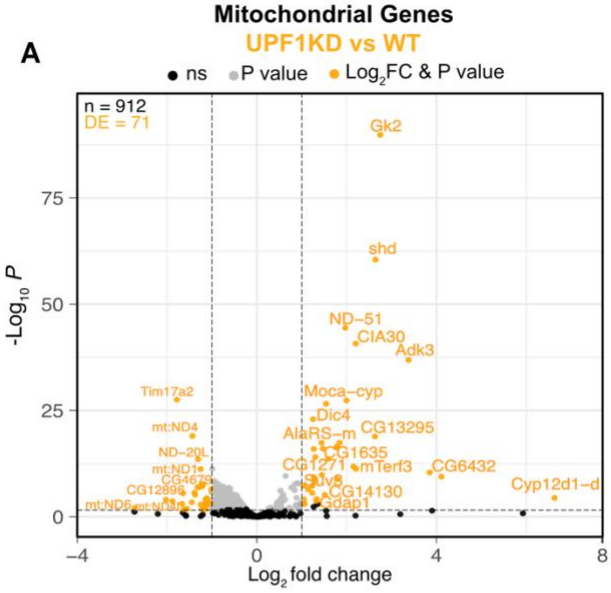

B

mtDNA genes UPF1KD *testes*

Gene Name	*Log$_2$ fold change*	*P value*	*P.adj*
mt:ATPase6	-0.655827550	2.40E-02	5.83E-02
mt:ATPase8	-1.577764833	6.50E-01	NA
mt:Col	**-1.023321635**	**9.45E-04**	**3.67E-03**
mt:ColI	**-1.142358752**	**5.20E-03**	**1.61E-02**
mt:ColII	**-1.066965999**	**2.85E-04**	**1.29E-03**
mt:Cyt-b	**-0.988657948**	**6.88E-03**	**2.05E-02**
mt:ND1	**-1.253831632**	**6.2E-12**	**8.97E-11**
mt:ND2	**-1.624695449**	**1.60E-02**	**4.19E-02**
mt:ND3	**-1.882212201**	**2.03E-04**	**9.52E-04**
mt:ND4	**-1.436011339**	**1.01E-19**	**2.51E-18**
mt:ND4L	**-2.026339133**	**9.92E-05**	**5.05E-04**
mt:ND5	**-0.857148137**	**1.88E-07**	**1.9E-07**
mt:ND6	**-2.720610040**	**8.25E-03**	**2.39E-02**
mt:lrRNA	-1.021457386	5.50E-02	1.13E-01
mt:srRNA	-1.364034250	1.11E-01	2.02E-01

C

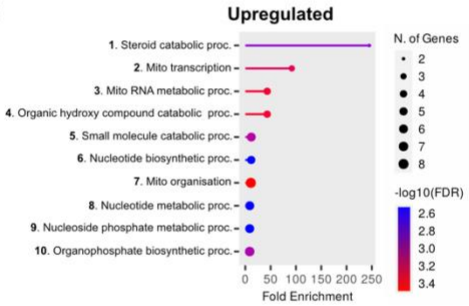

Pathway	*Genes*
1	*dare*, ***Cyp12d1-d***
2	*mtTFB2, Rim2*, ***mTerf3***
3	*Suv3, mtTFB2, Rim2*, ***mTerf3***
4	***Gk2***, *CG1271, dare*, ***Cyp12d1-d***
5	***CG9547***, ***Gk2***, *CG1271, CG5805, dare*, ***Cyp12d1-d***
6	***CG9547***, *CG5757, Ady43A, CG8080, dnk*
7	*CG9240, mtDNA-helicase, Gdap1*, ***CIA30***, *CG14130, Rim2, Top3alpha, ND-B8*
8	***CG9547***, *CG5757, CG1635, dnk, Ady43A, CG8080*
9	***CG9547***, *CG5757, CG1635, dnk, Ady43A, CG8080*
10	***CG9547***, *CG5757*, ***Gk2***, *CG1271, dnk, Ady43A, CG8080*

D

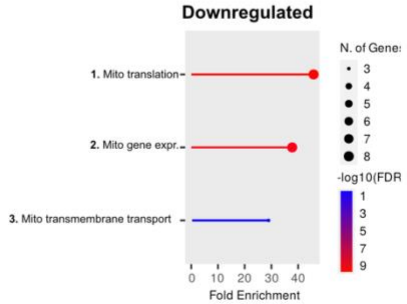

Pathway	*Genes*
1	*CG4679, mRpL34, tko, mRRF1, mRpS24, mRpL18, mRpL10, mRpL33*
2	*CG4679, mRpL34, tko, mRRF1, mRpS24, mRpL18, mRpL10, mRpL33*
3	***Tim17a2***, ***sea***, *mRpL18*

E

Genes involved in mtDNA transcription

Gene Name	*Log$_2$ fold change*	*P.adj*
mtRNApol	1.308010491	2.71E-17
TFAM	-1.197870253	1.99E-07
mtTFB2	1.513939599	4.58E-05
mTerf3	2.207713149	8.11E-11

F

Genes involved in the elimination of paternal mtDNA

Gene Name	*Log$_2$ fold change*	*P.adj*
EndoG	-0.9645613	5.25E-03
PolG1	1.24559368	7.45E-10

Figure 8. UPF1KD results in the downregulation of mtDNA-encoded genes in the spermatids. DESeq2 differential expression analysis of mitochondrial associated genes (n = 912), and mtDNA encoded genes (n = 15) in UPF1 vs. WT RNA-seq samples**.** Values were calculated based on a comparison of 23798 genes. **(A)** Volcano plot of DEGs associated with mitochondria, significant DEG (n = 71; 40 upregulated and 31 downregulated) are shown in orange (-1< LFC >1, P<0.05), grey indicates significant, but not highly misregulated genes (1> LFC >-1, P<0.05), and those in black are non-significantly changed (P>0.05). (**B**) A list showing mtDNA-encoded genes, gene name, LFC, P value and P.adj are shown. Downregulated genes, whereby P.adj <0.05, are shown in red. (**C-D**) Gene Ontology (GO) analysis of upregulated (**C**) and downregulated genes (**D**). Graph showing significantly enriched GO terms (left panel), the node size is determined by the number of genes associated with the given GO term, the colour corresponds to the -$\log_{10}$(FDR), from blue (lowest) to red (highest), only pathways where an FDR of <0.05 are shown. The different GO terms are ordered based on fold enrichment value. Pathways are numbered numerically, and misregulated genes involved in these pathways, are shown in the corresponding table (right panel), with genes identified as highly misregulated amongst all genes shown in bold. Upregulated GO terms: GO:0006706 (1), GO:0006390 (2), GO:0000959 (3), GO:190161 (4), GO:0044282 (5), GO:0009165 (6), GO:0007005 (7), GO:0009117 (8), GO:0006753 (9), and GO:0090407 (10). Downregulated GO terms: GO:0032543 (1), GO:0140053 (2) and GO:1990542 (3). Relative expression values of previously known genes involved in mtDNA transcription (**E**; blue) and elimination of paternal mtDNA from spermatids (**F**; pink), gene name, LFC and P.adj are shown.

Figure S11

A

UPF1KD vs Control

	Gene Name	Log_2 fold change	P value	P.adj
mtDNA genes	mtATPase6	-0.121669908	4.55E-01	7.48E-01
	mtATPase8	-1.736109965	3.25E-01	NA
	mt:CoI	**-0.241918765**	**1.79E-07**	**5.99E-06**
	mt:CoII	**-0.288249221**	**2.58E-07**	**8.32E-06**
	mt:CoIII	**-0.202789511**	**7.93E-05**	**1.38E-03**
	mt:Cyt-b	**-0.268682084**	**3.23E-07**	**1.02E-05**
	mt:ND1	-0.298109754	1.06E-02	7.60E-02
	mt:ND2	-0.555731377	5.46E-01	8.41E-01
	mt:ND3	-0.120528376	3.20E-01	6.80E-01
	mt:ND4	**-0.297717782**	**3.54E-04**	**4.89E-03**
	mt:ND4L	-0.613842504	6.90E-01	NA
	mt:ND5	**-0.268765505**	**2.27E-04**	**3.38E-03**
	mt:ND6	-0.07744984	9.89E-01	9.97E-01
	mt:lrRNA	-0.089955585	2.95E-02	1.63E-01
	mt:srRNA	-0.954116292	2.83E-01	6.40E-01
mtDNA transcription	mtRNApol	-0.156476785	1.30E-01	4.27E-01
	TFAM	-0.219988157	8.78E-03	6.61E-02
	mtTFB2	0.160574090	4.52E-01	7.80E-01
	mTerf3	**0.679519618**	**6.91E-05**	**1.22E-03**

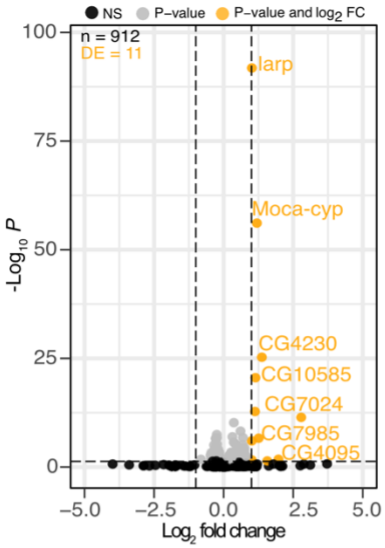

B

UPF2KD vs Control

	Gene Name	Log_2 fold change	P value	P.adj
mtDNA genes	mtATPase6	-0.126847832	7.50E-01	9.97E-01
	mtATPase8	0	1	NA
	mt:CoI	-0.116041509	4.93E-01	9.57E-01
	mt:CoII	-0.107803022	5.65E-01	9.73E-01
	mt:CoIII	-0.112439665	5.57E-01	9.72E-01
	mt:Cyt-b	-0.369023343	3.64E-02	3.26E-01
	mt:ND1	-0.079116890	6.42E-01	9.90E-01
	mt:ND2	-0.004918716	9.81E-01	9.99E-01
	mt:ND3	-0.090678381	6.68E-01	9.95E-01
	mt:ND4	-0.189041338	3.50E-01	8.97E-01
	mt:ND4L	-0.920115841	1.96E-01	1.51E-01
	mt:ND5	-0.128287318	5.15E-01	9.69E-01
	mt:ND6	-0.67681824	2.49E-01	8.21E-01
	mt:lrRNA	-0.059135865	7.59E-01	9.97E-01
	mt:srRNA	0.206396334	6.99E-01	9.95E-01
mtDNA transcription	mtRNApol	0.101694438	4.39E-01	9.57E-01
	TFAM	-0.227302625	1.18E-01	6.19E-01
	mtTFB2	0.300541961	3.37E-01	8.92E-01
	mTerf3	0.336219887	1.66E-01	7.19E-01

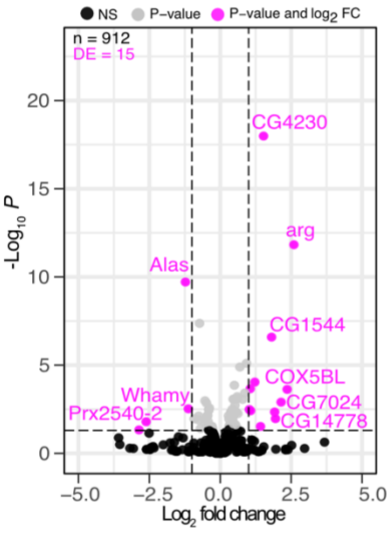

C

UPF3KD vs Control

	Gene Name	Log_2 fold change	P value	P.adj
mtDNA genes	mtATPase6	0.260797986	5.12E-01	7.71E-01
	mtATPase8	1.537316393	7.58E-01	NA
	mt:CoI	0.086500806	6.09E-01	8.31E-01
	mt:CoII	0.031366519	8.67E-01	9.53E-01
	mt:CoIII	0.056584767	7.68E-01	9.15E-01
	mt:Cyt-b	-0.164143368	3.52E-01	6.50E-01
	mt:ND1	0.257240300	1.31E-01	4.07E-01
	mt:ND2	0.343062765	9.23E-02	3.44E-01
	mt:ND3	0.378093948	7.37E-02	3.05E-01
	mt:ND4	0.172587123	3.93E-01	6.85E-01
	mt:ND4L	-0.310224989	3.83E-01	6.77E-01
	mt:ND5	0.233876038	2.35E-01	5.42E-01
	mt:ND6	-0.381893900	5.14E-01	7.72E-01
	mt:lrRNA	0.352963141	6.69E-02	2.89E-01
	mt:srRNA	0.569075046	2.85E-01	5.92E-01
mtDNA transcription	mtRNApol	0.081954581	5.82E-01	8.14E-01
	TFAM	-0.253056204	8.36E-02	3.26E-01
	mtTFB2	0.482089173	1.24E-01	3.98E-01
	mTerf3	0.132678358	5.89E-01	8.19E-01

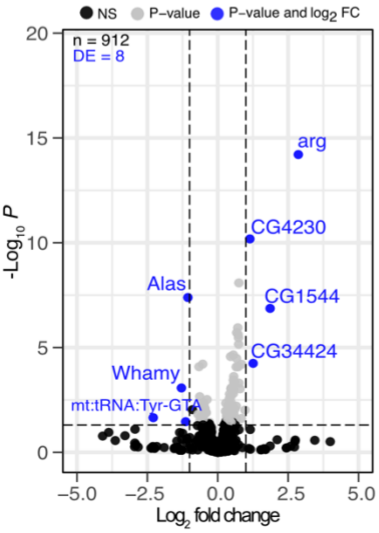

Figure S11. UPF1KD results in a reduced mtDNA genes expression in S2 cells. (**A**) DESeq2 differential expression analysis of mtDNA genes n = 15, values were calculated based on the comparison against 17610 expressed genes, in S2 cells. (**A**) UPF1KD, (**B**) UPF2KD and (**C**) UPF3KD (**D**) vs. control RNA-seq samples. Gene ID, LFC, P-value and the P.adj values are shown. Downregulated and upregulated genes associated with P.adj value of <0.05 are highlighted in red and green, respectively. For each panel, the list on the top shows mtDNA genes while that at the bottom the 4 nuclear genes involved in mtDNA transcription. The Volcano plots in the right of each panel indicate differentially expressed mitochondrial genes (-1< LFC >1, P<0.05) with coloured dots: in the UPF1KD (orange; 11 upregulated and 0 downregulated), in the UPF2KD (magenta, 11 upregulated and 4 downregulated) and UPF3KD (blue, 4 upregulated and 4 downregulated) grey indicates significant, but not highly misregulated (1> LFC >-1, P<0.05) and those in black are non-significant (P>0.05).

Figure S12

A Salivary Glands: *Fkh>UPF1$^{RNAi(1)}$ vs. WT*

	Gene Name	Log_2 fold change	P value	P.adj
mtDNA genes	mt:ATPase6	-1.064638193	2.17E-01	3.81E-01
	mt:ATPase8	-2.619035488	3.36E-01	NA
	mt:Col	**-1.507321801**	**1.37E-02**	**5.06E-02**
	mt:ColI	-1.421391473	6.99E-02	1.71E-01
	mt:ColIII	**-1.548656547**	**1.33E-02**	**4.95E-02**
	mt:Cyt-b	**-1.531484214**	**1.53E-02**	**5.49E-02**
	mt:ND1	-1.88941363	4.65E-02	1.27E-01
	mt:ND2	-1.661285833	3.38E-02	9.98E-02
	mt:ND3	-1.756886338	1.05E-01	2.28E-01
	mt:ND4	-1.651485544	3.97E-02	1.13E-01
	mt:ND4L	-2.184730294	1.31E-01	2.68E-01
	mt:ND5	-1.291950222	4.62E-02	1.26E-01
	mt:ND6	-1.71356677	NA	NA
	mt:lrRNA	**-1.689974479**	**1.52E-02**	**5.48E-02**
	mt:srRNA	-1.913230769	1.20E-01	2.50E-01
mtDNA transcription	mtRNApol	0.463359585	3.51E-01	5.25E-01
	TFAM	0.028570966	8.93E-01	9.40E-01
	mtTFB2	**0.789462328**	**1.01E-02**	**4.03E-02**
	mTerf3	**1.447082661**	**3.41E-11**	**1.02E-09**

B Salivary Glands: *Fkh>UPF2^{RNAi} vs. WT*

	Gene Name	Log_2 fold change	P value	P.adj
mtDNA genes	mt:ATPase6	1.2486244	1.48E-01	3.64E-01
	mt:ATPase8	2.014782085	4.20E-01	NA
	mt:Col	-0.182363269	7.65E-01	8.91E-01
	mt:ColI	0.208435539	7.90E-01	9.03E-01
	mt:ColIII	-0.167575538	7.89E-01	9.02E-01
	mt:Cyt-b	0.53358748	3.98E-01	6.43E-01
	mt:ND1	0.355431542	7.08E-01	8.63E-01
	mt:ND2	**2.429926173**	**1.64E-03**	**1.32E-02**
	mt:ND3	0.980146376	3.66E-01	6.16E-01
	mt:ND4	0.605066873	4.51E-01	6.89E-01
	mt:ND4L	**3.129284157**	**2.75E-03**	**2.01E-02**
	mt:ND5	0.948505689	1.43E-01	3.57E-01
	mt:ND6	2.678818176	NA	NA
	mt:lrRNA	0.287255186	6.80E-01	8.46E-01
	mt:srRNA	1.498542924	2.22E-01	4.66E-01
mtDNA transcription	mtRNApol	0.599232245	2.31E-01	4.75E-01
	TFAM	0.116294661	5.89E-01	7.87E-01
	mtTFB2	0.659475616	3.52E-02	1.40E-01
	mTerf3	**0.954073216**	**1.83E-05**	**2.90E-04**

C Salivary Glands: *Fkh>UPF3^{RNAi} vs. WT*

	Gene Name	Log_2 fold change	P value	P.adj
mtDNA genes	mt:ATPase6	-0.743827145	3.89E-01	6.47E-01
	mt:ATPase8	-1.611815403	5.54E-01	NA
	mt:Col	-0.70531211	2.31E-01	5.22E-01
	mt:ColI	-0.732260899	4.73E-01	4.90E-01
	mt:ColIII	-0.562854103	2.59E-01	7.13E-01
	mt:Cyt-b	-0.602721259	3.40E-01	6.02E-01
	mt:ND1	-1.140490023	2.29E-01	4.88E-01
	mt:ND2	-0.715083437	3.58E-01	6.19E-01
	mt:ND3	-1.010918687	3.51E-01	6.13E-01
	mt:ND4	-0.828623677	3.02E-01	5.66E-01
	mt:ND4L	1.410627975	1.88E-01	4.40E-01
	mt:ND5	-0.468465065	4.70E-01	7.10E-01
	mt:ND6	-0.62618999	NA	NA
	mt:lrRNA	-0.264192082	7.04E-01	8.65E-01
	mt:srRNA	-0.171519744	8.89E-01	9.56E-01
mtDNA transcription	mtRNApol	-0.150718440	7.56E-01	8.97E-01
	TFAM	-0.318688093	1.39E-01	3.68E-01
	mtTFB2	-0.423084207	1.91E-01	4.44E-01
	mTerf3	**0.934110515**	**2.27E-05**	**5.10E-04**

Figure S12. RNA-seq analysis indicates downregulation of mtDNA genes in UPF1KD salivary glands. DESeq2 differential expression analysis of mtDNA genes n = 15, and mtDNA transcription factors (*mtRNApol*, *TFAM*, mtTFB2 and mTerf3), values were calculated based on the comparison against 17284 genes in UPF1KD (A), UPF2KD (B), and UPF3KD (E). Gene Name, Log_2 fold change, P-value, and the P.adj values are shown. Downregulated and upregulated genes with an associated P.adj value of either <0.05 or ⩽0.05 are highlighted in green and red, respectively.